Literature correction?

Multicomponent Reactions

ROYAL SOCIETY OF CHEMISTRY

PAPER
Brenno A. D. Neto *et al.*
Revisiting Biginelli-like reactions: solvent effects, mechanisms, biological applications and correction of several literature reports

Check for updates

Revisiting Biginelli-like reactions: solvent effects, mechanisms, biological applications and correction of several literature reports†

Pedro S. Beck, [ID] [a] Arthur G. Leitão, [ID] [a] Yasmin B. Santana,[a] José R. Correa,[a] Carime V. S. Rodrigues,[a] Daniel F. S. Machado,[a] Guilherme D. R. Matos, [ID] [a] Luciana M. Ramos,[b] Claudia C. Gatto, [ID] [a] Sarah C. C. Oliveira,[c] Carlos K. Z. Andrade [ID] [a] and Brenno A. D. Neto [ID] *[a]

This study critically reevaluates reported Biginelli-like reactions using a Kamlet–Abboud–Taft-based solvent effect model. Surprisingly, structural misassignments were discovered in certain multicomponent reactions, leading to the identification of pseudo three-component derivatives instead of the expected MCR adducts. Attempts to replicate literature conditions failed, prompting reconsideration of the described MCRs and proposed mechanisms. Electrospray ionization (tandem) mass spectrometry, NMR, melting points, elemental analyses and single-crystal X-ray analysis exposed inaccuracies in reported MCRs and allowed for the proposition of a complete catalytic cycle. Biological investigations using both pure and "contaminated" derivatives revealed distinctive features in assessed bioassays. A new cellular action mechanism was unveiled for a one obtained pseudo three-component adduct, suggesting similarity with the known dihydropyrimidinone Monastrol as Eg5 inhibitors, disrupting mitosis by forming monoastral mitotic spindles. Docking studies and RMSD analyses supported this hypothesis. The findings described herein underscore the necessity for a critical reexamination and potential corrections of structural assignments in several reports. This work emphasizes the significance of rigorous characterization and critical evaluation in synthetic chemistry, urging a careful reassessment of reported synthesis and biological activities associated with these compounds.

Introduction

Today, there is no doubt about the significance of multicomponent reactions (MCRs) as essential tools within the synthetic organic toolbox. MCRs offer the potential to generate diversity, complexity, and quickly assemble libraries of bioactive compounds. They may also align with green principles and the prospect of sustainable processes. As recently highlighted,[1] however, solvent effects have often been overlooked in the context of MCRs. The presence of multiple (at least three) active reagents, various mechanistic steps, and the possibility of multiple mechanistic pathways render MCRs particularly susceptible to the influence of solvent effects.[2] The significance of solvent effects in all areas of chemistry is undeniable, as discussed in several reviews.[3–5] While no one disputes this importance, only a handful of studies have made dedicated efforts to unravel these fundamental and vital effects on MCRs.[6–11] If we delve into quantitative effects, the available studies are even more limited.[12–15] No one questions the importance of solvent screening for determining the optimal reaction conditions that promote chemical transformations and enhance productivities. But to advance the realm of MCRs, detailed investigations into solvent effects become paramount. As an illustration, we have recently demonstrated that a simple change in solvent, such as using methanol, can modulate the mechanism of the Ugi 4-component MCR, directing it towards an alternative catalytic cycle.[16]

Catalysis is regarded as a fundamental tool for aligning MCRs with the principles of green chemistry.[17] Considerable effort should be dedicated to achieving more efficient reac-

[a]*University of Brasilia, Institute of Chemistry, Laboratory of Medicinal and Technological Chemistry. Campus Universitário Darcy Ribeiro, Brasília, DF, 70910-900, Brazil. E-mail: brenno.ipi@gmail.com*
[b]*Universidade Estadual de Goiás (UEG), Anápolis, Goiás, 75001-970, Brazil*
[c]*University of Brasilia, Institute of Biology, Laboratory of Allelopathy, Campus Universitário Darcy Ribeiro, Brasília, DF, 70910-900, Brazil*

†Electronic supplementary information (ESI) available: Additional optimization experiments, copies of ¹H, and ¹³C{¹H} NMR, HRMS and IR spectra for all compounds. All computed structures, relative and absolute energies of all structures, reaction energy profiles, and Cartesian coordinates. CCDC 2323129. For ESI and crystallographic data in CIF or other electronic format see DOI: https://doi.org/10.1039/d4ob00272e

3630 | *Org. Biomol. Chem.*, 2024, **22**, 3630–3651

This journal is © The Royal Society of Chemistry 2024

tions, bypassing the use of hazardous and toxic solvents, minimizing waste, and exploring both efficient and convenient purification methods. While MCRs possess inherent environmentally friendly qualities, there is still a substantial need for scientific endeavors to advance sustainable processes.[18–20] The path toward greener catalyzed MCRs is illuminated by the elucidation of solvent effects, which also play a crucial role in considerations of selectivities (enantio- and diastereoselectivity), mechanistic route selection, and the recovery of catalytic systems.[1] Given that several solvents that were previously used are now subject to stricter regulations worldwide,[21–25] it is imperative to replace such solvents with environmentally friendly, bio-based, and non-toxic alternatives.[26–32] This replacement commences by utilizing solvents that possess these desirable features in basic research.[33–36]

The Biginelli reaction stands as one of the most extensively studied MCRs.[37] Discovered in 1891 by Pietro Biginelli,[38] this reaction has been a subject of ongoing debate and discussion. In several reports, there are discrepancies, such as the year of discovery being noted as 1893, when, in fact, it was in 1891, and two years later, Biginelli published the comprehensive accounts of his eponymous reaction.[38] Another intriguing aspect is that the original structure proposed by Biginelli himself was not a heterocyclic compound but an open structure that required revisitation (see Scheme 1).

More recently, the reaction has been carried out under the so-called "catalyst-free" conditions, but the beneficial effect and importance of catalysis have been indisputably demonstrated for the Biginelli MCR.[13] Since then, no "catalyst-free" condition has been advocated. This "catalyst-free" issue is particularly curious, considering that the advantages of catalysis for conducting this MCR had already been described since the original Biginelli reports at the end of the 19th century.[39–42] The mechanism of the reaction is still a topic of intense debate, with three different routes currently proposed to explain this MCR.[43] This indicates that controversies continue to be associated with the Biginelli multicomponent transformation.
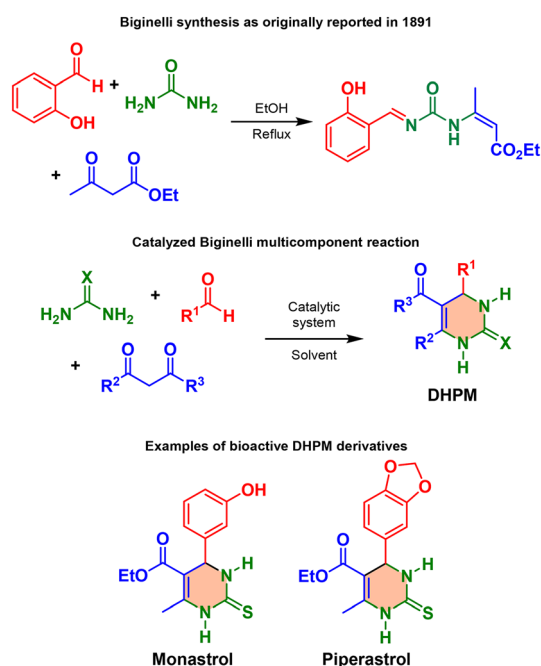
A groundbreaking study[44] has revealed the remarkable biological activity of a Biginelli adduct, specifically a DHPM (3,4-dihydropyrimidin-2(1H)-one or -thione derivative) known as Monastrol (see Scheme 1). Monastrol demonstrated the ability to inhibit the mitotic kinesin Eg5, a motor protein crucial for spindle bipolarity, ultimately leading to the formation of monoastral spindles in mitotic cells and subsequent cell death. This discovery has fueled the development of numerous DHPM derivatives, most of which are in racemic form and are synthesized directly through the Biginelli MCR. These derivatives exhibit potent antitumoral activities, as documented elsewhere.[45–55] The wide range of biological properties associated with DHPMs has been comprehensively reviewed.[56–58]

Because of the appealing biological activities observed in various DHPM derivatives,[59] their straightforward synthesis, and the rapid generation of libraries of bioactive compounds, variations of the Biginelli reaction, often referred to as Biginelli-like (or Biginelli-type) reactions, have been documented and extensively reviewed.[60–66] These adaptations of the Biginelli reaction encompass a range of strategies that involve modifying a specific reagent among the three components or replacing one (or two) of them,[67–77] as illustrated by a few examples in Scheme 2. Much like the Biginelli reaction, these variations also exhibit their unique characteristics, including distinct mechanistic pathways and others. However, these variations also exhibit enduring polemic issues.
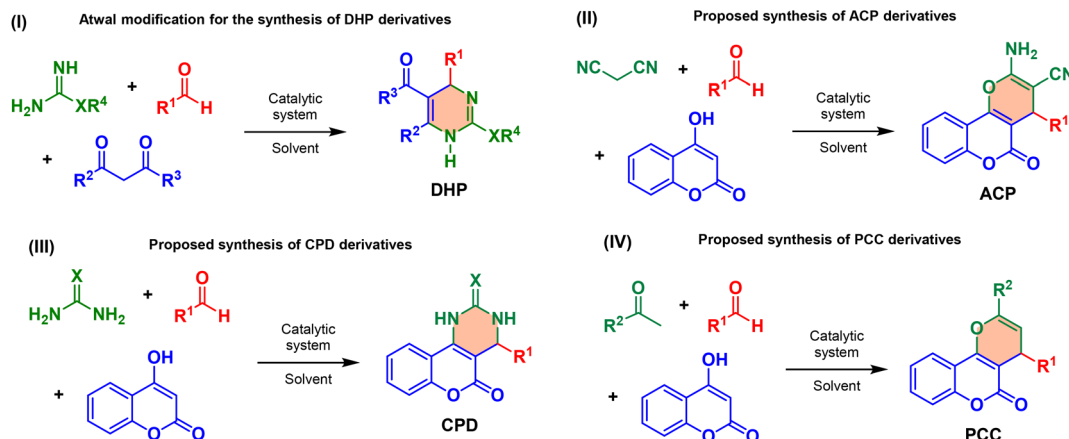
In this study, we present our findings concerning solvent effects on Biginelli-like MCRs, the mechanistic pathways of these transformations, and associated side reactions. We also advocate for a comprehensive correction of the vast existing literature on this topic. Within this context, we demonstrate that certain structures attributed to MCRs have been inaccurately assigned. Given that these structures are currently employed in biological evaluations, yielding distinct yet positive effects, there is an urgent need for their reassessment.

Scheme 1 From top to bottom: the original synthesis and structure initially proposed for the first reported Biginelli reaction, the presently accepted Biginelli MCR, and examples of bioactive derivatives (dihydropyrimidin-2(1H)-thiones – DHPMs) directly obtained through the Biginelli MCR.

Results and discussion

Our investigation employed various analytical techniques and models, including Kamlet–Taft solvent descriptors, NMR analysis, IR spectroscopy, single-crystal X-ray analysis, high-resolution mass spectrometry, and DFT calculations. These analyses have exposed a significant issue within the scientific literature, necessitating an immediate clarification and rectification of these studies.

This journal is © The Royal Society of Chemistry 2024

Org. Biomol. Chem., 2024, **22**, 3630–3651 | **3631**

Scheme 2 Examples of Biginelli-like multicomponent transformations: (I) 1,4-dihydropyrimidine (DHP) synthesis,[78–81] (II) 2-amino-3-cyano-4*H*-pyrans (**ACP**) derivatives,[82,83] (III) 3,4-dihydro-2*H*-chromeno[4,3-*d*]pyrimidine-2,5(1*H*)-dione or thione (**CPD**) derivatives,[82,84–102] and (IV) pyrano[3,2-*c*]chromen-5(4*H*)-ones (**PCC**) compounds.[103–106]

We initiated the assessment of solvent effects using a model reaction for the synthesis of **CPD** derivatives (Scheme 2-III). Equimolar amounts of urea, 4-hydroxycoumarin, and benzaldehyde were employed as starting reagents to produce **CPD-01** (with X = O and R^1 = Ph, as shown in Scheme 2-III). In pursuit of more sustainable catalytic approaches, we selected a superacid imidazolium-based ionic liquid known for its high activity in MCRs[107] (see Scheme S1 and Table S1 in the ESI† for the structure of the catalyst MSI₃PW). Ionic liquids are currently regarded as sustainable alternatives in various industrial processes, as extensively reviewed elsewhere.[108] These organic salts have been utilized in the chemical industry as solvents and catalysts for nearly two decades,[109] and their environmentally friendly and advantageous physicochemical properties, combined with their customizable characteristics, justify the increasing industrial interest in using these compounds as alternatives to toxic and hazardous solvents or catalysts.[110–115]

The reaction conditions were subsequently optimized in water as the solvent, considering various parameters such as temperature, catalyst amount, and reaction time (see Fig. S1†) to synthesize **CPD-01**. The optimal conditions were established as follows: 1.00 mmol of each reagent, 0.5 mL of the solvent, 5 mol% of the catalyst, 80 °C, and a reaction time of 60 min. Table S1† provides a summary of the results obtained. During the reaction, a solid precipitated, which could be purified by washing it with a mixture of ethanol and water (1 : 1 v/v). The solid was subsequently dried and initially characterized by its melting point, yielding a value in the range of 160–162 °C. The literature, however, contains various different values for the melting point of **CPD-01** (as shown in Table S2† and Fig. 1), prompting us to investigate the underlying reasons for this discrepancy. As recently discussed in the context of MCRs,[116] melting point characterizations can potentially lead to erroneous conclusions when not supported by additional analyses.

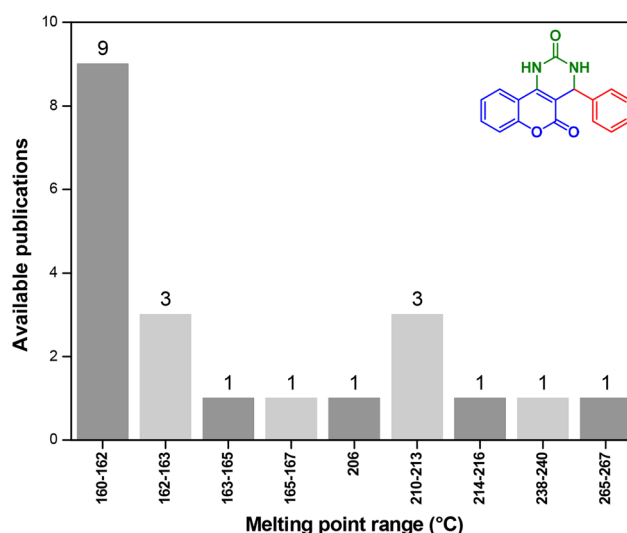Eleven different solvents, including some toxic solvents for gauging a wide range of Kamlet–Abboud–Taft

Fig. 1 Melting points descriptions for the claimed structure of **CPD-01**. See Table S2† for the references.

parameters,[117–120] were initially tested under the optimized conditions (Table S1†) to depict mechanistic information, but with no intention to use them as solvents for this MCR after reaching a greener condition. Reactions requiring excess reagents were also tested only to gain knowledge on the solvent effects over the reaction mechanism (Fig. S2†), but our goal was to establish an appropriate reaction condition to avoid any excess and aiming at reaching the lowest possible *E* factor (Table S1†).[121–123]

In the Biginelli MCR[38] (Scheme 1), a 1,3-dicarbonyl reagent is typically employed (*e.g.*, ethyl or methyl acetoacetate).[124–135] This reagent is reactive in its enol tautomeric form, but not in the diketo form, as demonstrated in the catalyzed (HCl 10%) version disclosed in the groundbreaking publication by Sherwood and co-workers.[12] Catalyst-free versions, conducted in alternative green solvents, follow the same trend, where

3632 | *Org. Biomol. Chem.*, 2024, **22**, 3630–3651

This journal is © The Royal Society of Chemistry 2024

only the enol tautomeric form is reactive, as demonstrated by us[13] and others.[15] In these cases, the dipolarity/polarizability ($\pi^\star$) was the Kamlet–Taft (KT) descriptor with the most significant influence on the reaction outcome, particularly on achieving higher productivities. This is because the concentration of the enol tautomeric form dictates the final yields. Therefore, the application of a solvent with low values of $\pi^\star$ (such as *p*-cymene as a green alternative)[12] was crucial for restoring the reactive enol tautomeric form and advancing the MCR.

In the current evaluated Biginelli-like reaction, the "key reagent" (*i.e.*, 4-hydroxycoumarin) is predominantly found in its enol tautomeric form to sustain the conjugated (aromatic) structure of the molecule, which is considerably more stable.[136] The enol tautomeric form is found almost exclusively, regardless of both the solvent used and its Kamlet–Taft parameters, and this is why this reagent is known for displaying good-to-excellent nucleophilic character.[137–139] This aspect circumvents the reactivity issue and expands the opportunity to explore several other solvents. The three tautomeric forms of 4-hydroxycoumarin have been thoroughly reviewed elsewhere.[140]

The three possible and proposed mechanisms of this Biginelli-like transformation (Scheme 3) already available[88–91,93,141] (and some close variants[82,142,143]) could in principle help to understand the observed solvent effects, although no experimental evidence has been so far provided for this specific MCR transformation to the best of our knowledge.

Following the principles of organic chemistry transformations, it is reasonable to exclude the enamine pathway (see Scheme 3) without the need for further investigation. This is particularly evident because the enol tautomer is predominantly present. Notably, the Kamlet–Taft β parameter emerges as the primary solvent descriptor that influences the rate of the Knoevenagel condensation, as documented in the existing literature.[144] Upon examining Table S1 (and Fig. S2†), it becomes apparent that higher values of α promote product formation, thus implying the iminium pathway as the preferred route for **CPD** formation, rather than the Knoevenagel route typically associated with solvents characterized by high β values. In another study,[145] it was indicated that depending on
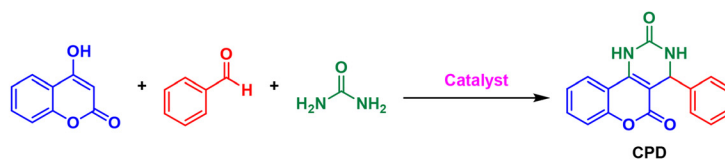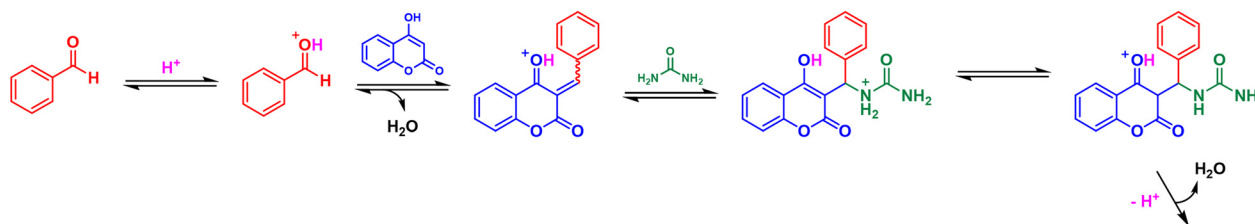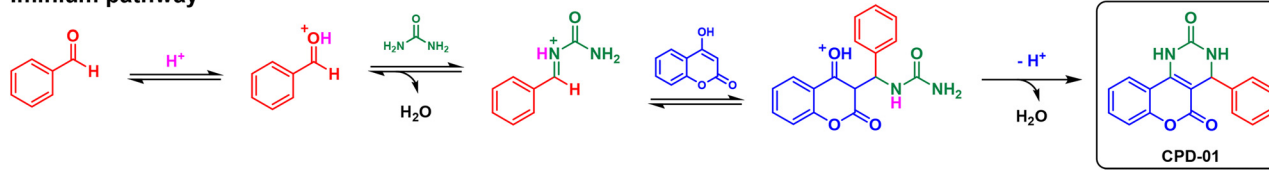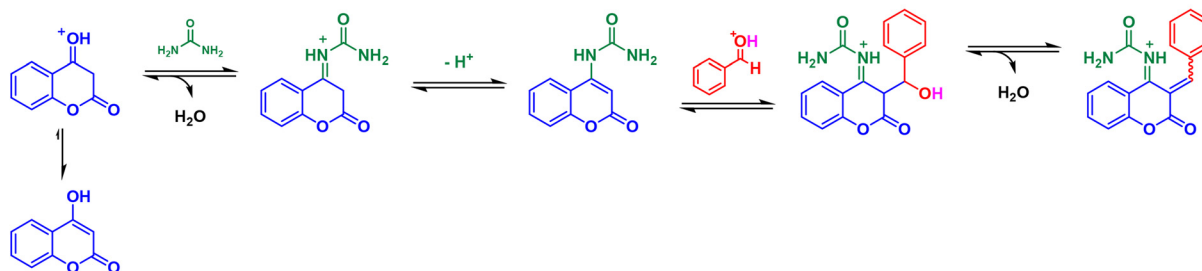

Scheme 3 Three previously proposed reaction pathways for the Biginelli-type reaction studied herein which provide plausible explanations for **CPD-01** formation under acidic catalytic conditions.

the catalytic conditions, π^* was identified as the key Kamlet–Taft parameter, and low-polarity solvents performed better. However, α showed no discernible correlation.

On the surface, the results from our experiments may appear logical and promising in elucidating the transformation (Table S1 and Fig. S2†). However, a study[12] has previously demonstrated that the values of the α descriptor are generally statistically insignificant in terms of Biginelli reaction productivity. As a result, the findings presented here appear to contradict the expected behavior derived from a robust solvent effect model, therefore making our results highly questionable. The literature[12,144,145] has indeed highlighted both β (favoring Knoevenagel condensations) and π^* (favoring the iminium route) as critical descriptors for this transformation or for the formation of any key intermediate (i.e., the iminium or the Knoevenagel intermediates). However, our findings contrast with these published and well-conducted works, as we identify α from the Kamlet–Taft parameters as the primary factor influencing productivity in the synthesis of **CPDs**.

At this juncture, a comprehensive analysis of the results and a comparison with the existing literature became imperative. NMR (^{1}H and ^{13}C, as shown in Fig. S3†), revealed certain issues. Notably, the chemical shifts in the NMR, especially for the benzylic hydrogen, were excessively deshielded (exceeding 6.00 ppm when it should be approximately 4.00 ppm). Additionally, while one would anticipate 15 carbon signals, only 14 were observable, potentially due to the overlapping of one of the aromatic signals. High-resolution electrospray (tandem) mass spectrometry analyses – ESI-MS(/MS) – were conducted and yielded no signals corresponding to the expected ionic species with a m/z of 293 (for the protonated **CPD-01**). We also attempted both high resolution MALDI and EI ionization methods to detect signals of m/z 293 (for MALDI) or m/z 292 (for EI), but these procedures were unsuccessful. As a final effort, elemental analyses were undertaken to determine the composition of the sample and compare it with the literature. The results indicated a low content of nitrogen, significantly below what was expected for the claimed structure of **CPD-01** (Table S3†). To ensure the reproducibility of these results, several **CPD** derivatives (see Scheme S2†) were synthesized and analyzed. All of these data are presented in Table S3 and are compared with the available literature (please refer to the cited references and the ESI†). In our assessment, however, the data did not align with the claimed structures of the **CPD** derivatives.

To explore the events unfolding during the reaction, we monitored it using ESI-MS(/MS), a technique renowned for its effectiveness in tracking MCRs.[43] This method stands out for its capability to provide continuous snapshots of the solution phase, to facilitate a gentle transfer to the gas phase, and detect transient intermediates and adducts.[146–149] In this work, we also employed an aldehyde derivative with a charge tag in its structure to enhance detection and prevent the escape of any intermediate during the reaction (Fig. S4–S6†). This approach is recognized for enhancing signal-to-noise

ratios in ESI analyses and enabling a more comprehensive monitoring of catalyzed reactions.[150] Comparable outcomes were noted when employing benzaldehyde instead of the charge-tagged aldehyde (Fig. 2).

During the reaction monitoring (Fig. 2), notable signals include the protonated aldehyde of m/z 107, the protonated coumarin of m/z 163, the Knoevenagel intermediate of m/z 251, the bisureide derivative of m/z 209 (from the iminium ion of m/z 149), and the presence of a dicoumarol derivative (m/z 413 and 435 for the sodiated derivative). Of interest is the ion of m/z 333 (sodiated) related to an advanced intermediate, from which cyclization should occur to yield the final MCR adduct, i.e., the **CPD-01**. No other discernible ions related to potential intermediates (Scheme 3) were observed. All attempts to observe the **CPD** derivative, both with and without a charged-tagged aldehyde, were unsuccessful.

At this point, it became evident that the reaction did not progress towards the formation of **CPD** scaffolds, not even through a concurrent mechanism (iminium- or Knoevenagel-like, as illustrated in Scheme 3). Under the tested conditions (Table S1†), it seemed that only dicoumarol derivatives (**DCs**) were actually being produced (Scheme 4). The synthesis failure of **CPD** derivatives, previously mentioned in the literature[151] but unexplored, resulted in the formation of only a **DC** derivative. It also elucidates our results from elemental analysis (Table S3†), indicating that the low nitrogen content arises from urea contamination. The difference between the calculated and obtained values for nitrogen content is indeed significant, as shown in Table S3.† It does not account, however, for the nearly perfect match of the CHN content described in the literature for some reports (see Table S7† for the references).

These results also contribute to explaining the diversity of melting points described (see Fig. 1 and Table S2†), indicating varying urea content as a contaminant of the claimed **CPD-01**, which was indeed **DC-01**. In due course, we will revisit the Kamlet–Taft analysis for this reaction. But we can anticipate that the formation of the **DC** derivative accounts for the significance of the α descriptor. In attempting to replicate numerous previously reported conditions for the **CPD** synthesis (see details in the Experimental section), we consistently obtained the **DC** derivative. Intriguingly, one of these reports describes an enantioselective **CPD** synthesis with high enantiomeric excess (ee) values, employing L-proline as the chiral catalyst. The lack of accessible HPLC (or GC) for ee confirmation, coupled with the presented NMR spectra, however, consistently supports the identification of nonchiral **DC** derivatives.

Simultaneously, our attempts to obtain **PCC**, **ACP** (see Scheme 2) and other Biginelli-like derivatives were ongoing. Despite some differences that we will elucidate in due course, we predominantly obtained only the **DC** derivative. These results point to a notable concern in the scientific literature regarding Biginelli-like reactions, predominantly when 4-hydroxycoumarin is involved as one of the components.
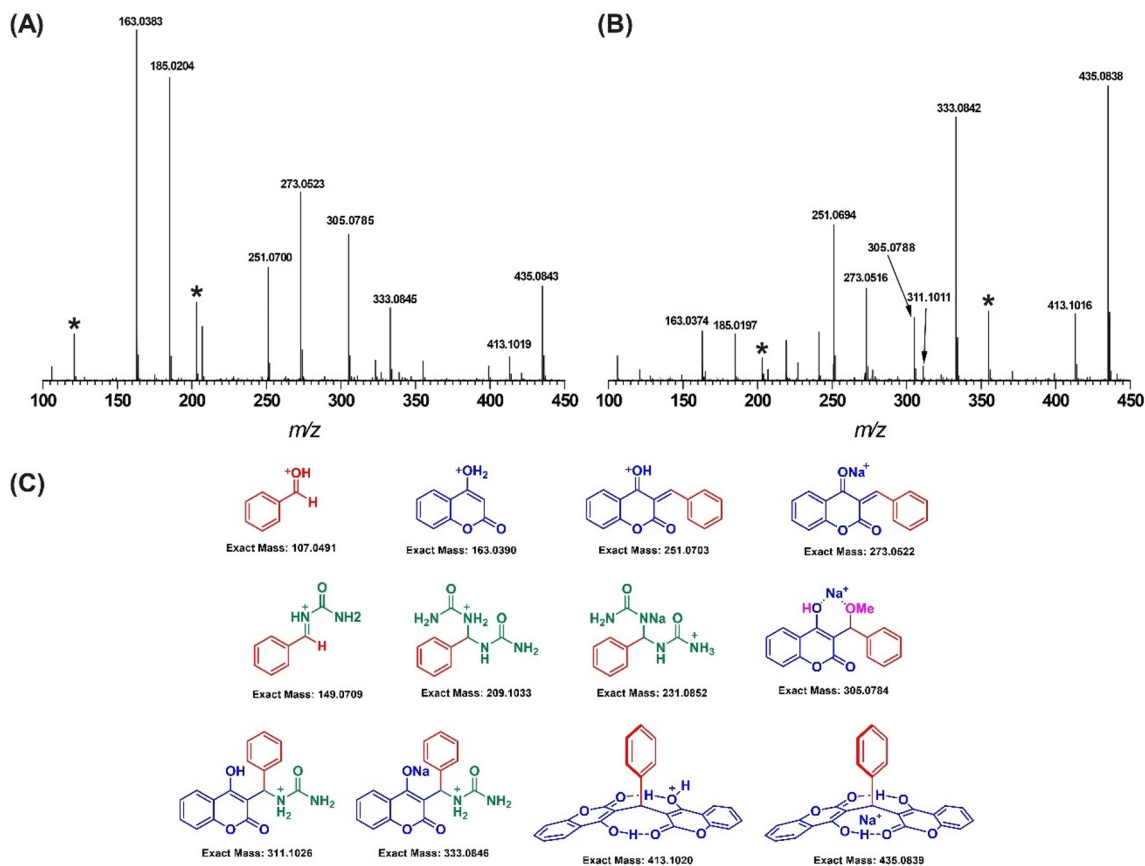
3634 | *Org. Biomol. Chem.*, 2024, **22**, 3630–3651

This journal is © The Royal Society of Chemistry 2024

Fig. 2 ESI(+)-MS(/MS) monitoring of the MCR employing benzaldehyde, urea and 4-hydroxycoumarin. (A) 5 min of reaction. (B) 45 min of reaction. (C) Detected structures and their calculated exact mass. Signals of *m/z* 209 and 231 are of very low intensities. The ion of *m/z* 305 corresponds to the reversible addition of a methanol molecule in the gas phase. The asterisk denotes fragments from other ions.
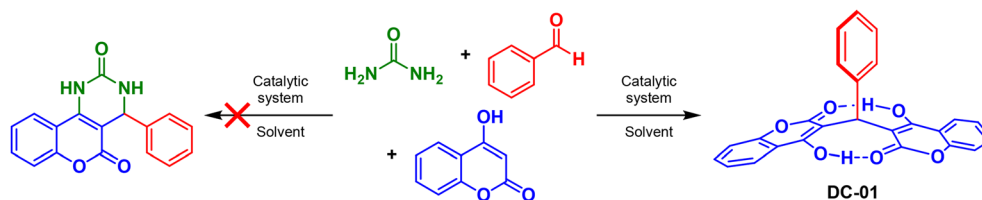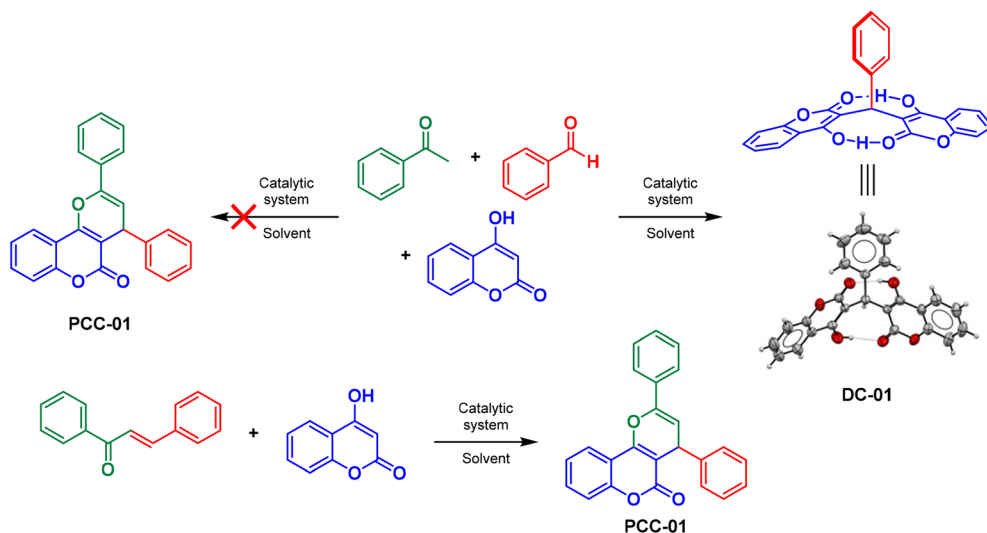

Scheme 4 Attempts to form **CPD-01** only resulted in the dicoumarol derivative **DC-01**, which was isolated but contaminated with urea. Several catalytic conditions were tested and their details are provided in the Experimental section and Table S1.†

The situation regarding **PCC** derivatives was particularly concerning, notably because the derivative **PCC-01** (R^1 and R^2 = Ph, Scheme 2) has been previously reported from a few authentic bimolecular reactions,[152–159] and the comprehensive characterization of this derivative was readily available. Despite our efforts, all attempts to obtain **PCC** derivatives in an MCR fashion (see Table S8†) were unsuccessful, yielding only **DC-01** in all attempts (Scheme 5). Interestingly, in one of the trials, a crystal suitable for X-ray analysis formed in the reaction medium, and **DC-01** was obtained in high yield and undoubtedly characterized. All available spectra (including spectroscopic descriptions) from the three-component reaction to

form **PCC-01** (see references in Scheme 2) are identical to **DC-01**, indicating a structural misassignment.

The case of **ACP** derivatives[160–162] yielded promising results. Despite the extensive volume of approximately 250 references detailing the MCR formation of **ACP** derivatives, and the laborious task of scrutinizing each of them, we found alignment with the **DC** structure description in only a few instances (as cited in Scheme 2). In a few other cases, the available characterizations did not allow for a more precise conclusion. This singular convergence indicates a degree of reliability in the characterization of this particular MCR class of compounds involving a coumarin as one of its components. For this multi-

This journal is © The Royal Society of Chemistry 2024

Org. Biomol. Chem., 2024, **22**, 3630–3651 | **3635**

Scheme 5 MCR attempts to form **PCC-01** only resulted in the dicoumarol derivative **DC-01**. **PCC-01** can be obtained through known bimolecular reactions. **DC-01** was obtained by mixing 1.00 mmol of each reagent, 5 mol% MSI$_3$PW (catalyst), in 1 mL of the selected solvent at 80 °C for 60 min. The bimolecular version of the reaction was carried out under stirring by mixing 1.00 mmol of each reagent and heating the mixture in a sealed flask for 3 h at 120 °C.

component synthesis, however, we observed a pH dependence. In our experiments, we observed a preference for **ACP-01** formation under basic conditions, whereas under acidic conditions, the **DC-01** derivative was preferentially obtained (Scheme 6).

Scheme 6 also depicts a reaction in which 5,5-dimethyl-1,3-cyclohexanedione was employed as the third component, resulting in the preferential formation of the desired multicomponent adduct **TCC-01**. Although a small amount of **DC-01** was also generated, it could be readily removed through recrys-
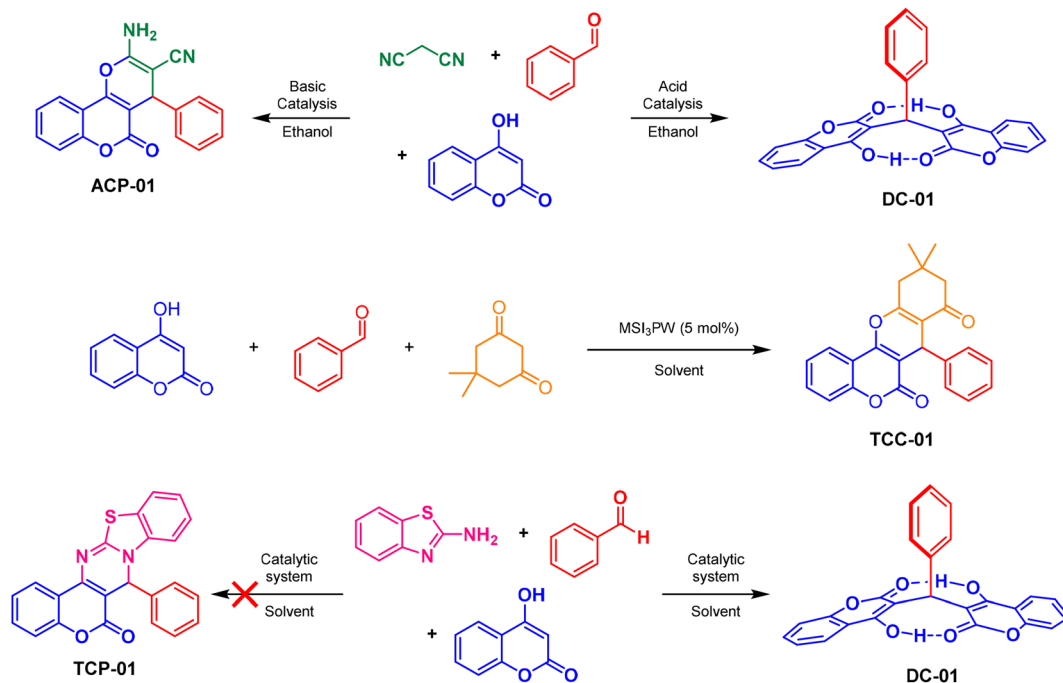
Scheme 6 (Top) Concurrent formation of **ACP-01** and **DC-01** depending on the catalytic conditions. For example, using 1.0 mmol of each reagent, EtOH as the solvent, and HCl (10 mol%) or MSI$_3$PW (5 mol%) as the catalytic system, **DC-01** is formed in 81% yield (considering 0.5 mmol of the coumarin) in 30 minutes at 80 °C. By switching the catalyst to *t*-BuOK, **ACP-01** is obtained in 70% yield. (Center) Preferential formation of **TCC-01** (10,11-dihydrochromeno[4,3-*b*]chromene-6,8(7*H*,9*H*)-dione derivative) under acidic conditions at 80 °C in water for 2 h. (Bottom) Preferential formation of **DC-01** (1.0 mmol of each reagent), EtOH as the solvent, and SLS (10 mol%) or MSI$_3$PW (5 mol%) as the catalyst, with no **TCP-01** obtained.

3636 | *Org. Biomol. Chem.*, 2024, **22**, 3630–3651

This journal is © The Royal Society of Chemistry 2024

tallization during the purification step of **TCC-01**. This result confirms the accuracy of the literature's description[163] regarding the formation of **TCC** derivatives through a multicomponent approach, with **DC-01** observed by us as a byproduct formed in small amounts.

A comparable multicomponent Biginelli-like reaction, wherein 2-aminobenzothiazole substitutes the 4-hydroxycoumarin, has also been documented in the literature.[84,164–169] Despite our attempts to reproduce various conditions for synthesizing the MCR adduct (Scheme 6), all efforts yielded **DC** derivatives, even when attempting to replicate the documented literature conditions, no **TCP** was obtained. Analysis of the available NMR spectra (or spectral descriptions) strongly suggests the formation of **DC** rather than any other MCR adduct.

Considering all these findings, we decided to explore conditions for synthesizing **CPD-01**. In this context, one of our objectives became to exploit the solvent effect to prevent the formation of the **DC-01** derivative by the second coumarin addition. This involved facilitating the addition of urea to the Knoevenagel intermediate (Scheme 3) or promoting the addition of coumarin to the iminium intermediate (Scheme 3). These efforts aimed at favoring the formation of the advanced intermediate through either of these two reaction pathways (Scheme 3). Subsequently, the advanced intermediate could undergo cyclization, ultimately resulting in the synthesis of **CPD-01**.

This situation is indeed unusual, as typically, conditions are sought to improve yields and selectivities rather than lower them. In this case, however, the lower the yield of the **DC** derivative, the better. Although we had previously ruled out the enamine pathway (Scheme 3), ironically, it is now the condition we aim to favor. The final cyclization step or an initial urea addition to the coumarin could, in principle, align with our goal of obtaining **CPD-01**, even though it is now dependent on the keto form of the coumarin reagent, which is found in a neglected concentration, as we discussed earlier in this work. The results from this solvent exploration are shown in Table 1.

Results from Table 1 revealed intriguing patterns. Solely by accounting for the solvent effect (Fig. 3), a significant drop in yield, from 95% (Table 1, entry 9) to 1% (Table 1, entry 24), was observed, aligning with our expectations. The most effective solvents in reducing **DC-01** formation were those with low values of β descriptors (see Table S9†) because high values of β tend to favor the coumarin addition followed by water elimination (Knoevenagel condensation). Our results now align with the literature,[144,145] as low values of β led to low yields of **DC-01**, as intended, reaffirming the significance of the solvent in favoring a specific reaction pathway. Fig. 4 initially shows that the β descriptor alone, however, has little significance in the reaction outcome for obtaining **DC-01**, and this correlation is not statistically significant for any reaction condition evaluated in this work.

The analysis of π^* does indicate a relatively significant correlation in the synthesis of **DC-01**. This parameter also reflects the solvent's ability to aid in the stabilization of charges or

Table 1 Solvent screening aimed at reducing **DC-01** formation. Reactions were carried out using 4-hydroxycoumarin (2.0 mmol) and benzaldehyde (1.0 mmol), MSI₃PW (5 mol%), 1.0 mL of the solvent, and 60 min

Entry	Solvent	Yield (%)	Entry	Solvent	Yield (%)
1	—	87	13	MeCN	36
2	H_2O (catalyst-free)	61	21	1,4-Dioxane	27
3	H_2O	93	15	CH_2Cl_2	27
4	EtOH	86	16	THF	26
5	BMI·PF₆	85	17	Triethylamine	26
6	BMI·NTf₂	85	18	Toluene	19
7	MeOH	72	19	AcOEt	18
8	t-BuOH	67	20	Hexane	14
9	BMI·BF₄	95	14	Limonene	13
10	n-OcOH	59	22	Cyclohexane	11
11	Acetone	59	23	CHCl₃	11
12	CF₃CH₂OH	52	24	p-Cymene	1–5[a]

Yields below 20% were arbitrarily highlighted. [a] Experiment repeated several times.

dipoles. Considering the protonation of reagents and the presence of polar intermediates in the reaction conducted under acid catalysis, this descriptor should be taken into account in synthesizing **DC-01** through a double coumarin addition to the aldehyde, *via* the formation of a Knoevenagel intermediate. Table 1 also shows that the best results are obtained in solvents with π^* ranging from middle to high values.

The α descriptor returned a relatively significant correlation (Fig. 3 and Table 1). For all good yields, however, solvents had relatively high values of α. Water, with the highest α value among all tested solvents, produced the desired product in one of the highest yields and under the most appropriate conditions, *i.e.*, using no reagent excesses. The presence of polar reagents/intermediates capable of solvent-solute interactions through hydrogen bonds and the stabilization of charged intermediates in an acidic medium also shed some light on the observed effect. The literature suggests that Michael additions are favored by high values of α,[170] and the second step for **DC** formation involves a Michael addition to the Knoevenagel intermediate. Another study[171] suggests that α and β play a role in this type of addition in a polymerization reaction.

In this context, the formation of **DC** relies on a combination of several factors, where α, β, and π^* contribute to improved yields. The β descriptor facilitates Knoevenagel formation (initial stage), while α also aids in the Michael addition (last stage). The π^* descriptor is recognized to influence the nucleophile reactivity in these reactions. However, in the present case, coumarin does not appear to be significantly affected, but rather, the stabilization of intermediates and transition states (TSs) seems to play a role. A multivariate analysis was then conducted, clearly demonstrating the importance of considering all three parameters, as depicted in Fig. 3D.

Now, back to our endeavors to synthesize **CPD-01**, in an effort to leverage the temperature effect, we opted for
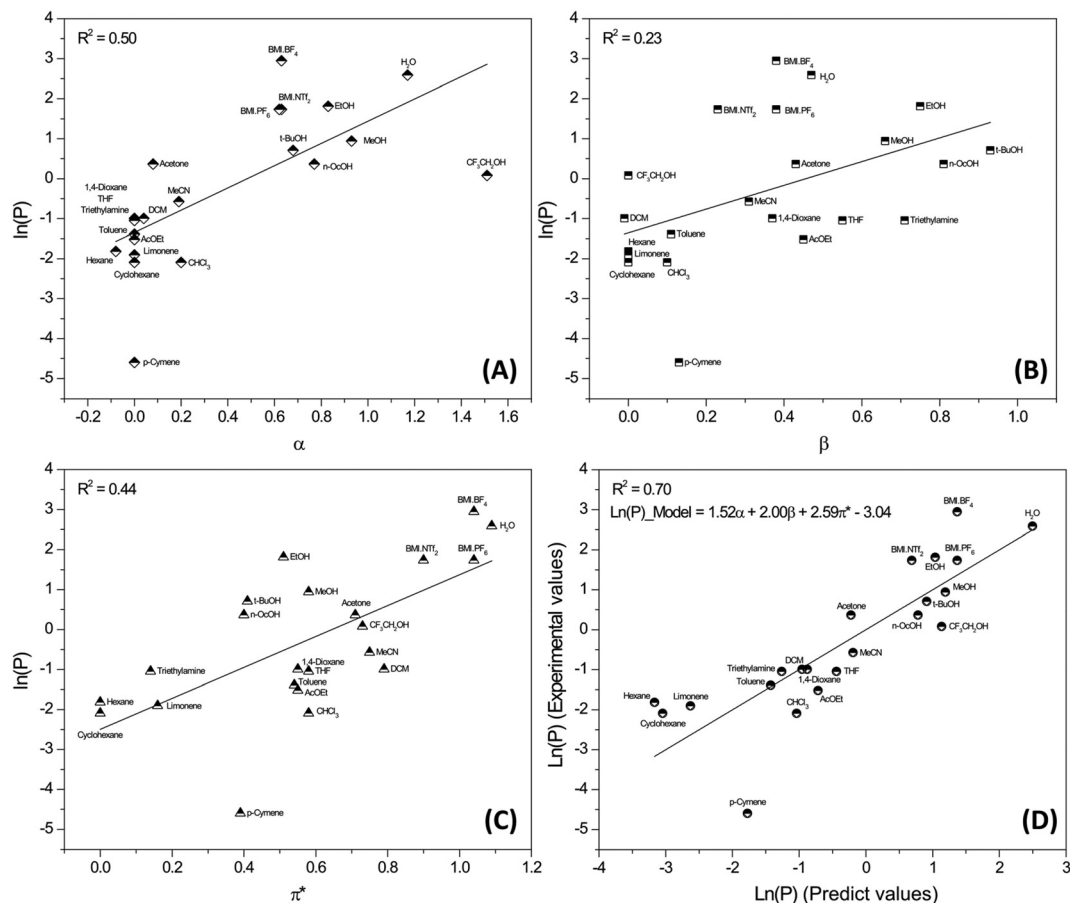
This journal is © The Royal Society of Chemistry 2024

Org. Biomol. Chem., 2024, **22**, 3630–3651 | **3637**

Fig. 3 Correlations of reaction productivity (expressed as ln(P)) as a function of the Kamlet–Taft parameters: (A) α, (B) β, (C) π^* and (D) multivariate correlations considering α, β and π^*. All data pertain to the isolated yields of the model reaction for **DC-01** formation (benzaldehyde and coumarin mixtures, 5 mol% of the catalyst MSI$_3$PW at 80 °C for 60 min).

p-cymene and limonene as solvents (low values of β), given their high boiling points. Despite conducting reactions in the temperature range of 80–140 °C, **CPD-01** formation was not observed at all. Utilizing p-cymene as the solvent, we employed ESI-MS(/MS) reaction monitoring with a charge-tagged aldehyde to observe the heterocyclic formation (Fig. 4). While **DC-01** formation was avoided for a period of time, no **CPD** was detected. Similar outcomes were noted with limonene as the solvent (Fig. S4 and S5†). We also explored reactions by employing 4-hydroxy-6-methyl-2-pyrone as the reagent instead of 4-hydroxycoumarin (Fig. S6†), but only the advanced intermediate could be detected, not the final MCR adduct.

The reaction was initiated by mixing the charge-tagged aldehyde and urea to promote the iminium ion formation while avoiding the Knoevenagel adduct. As shown in Fig. 4, this strategy proved effective, favoring the bisureide derivative of m/z 266 formed through the second urea addition to the aldehyde. This aligns with literature[12] findings that indicate a preference for the iminium pathway when p-cymene is the solvent. Following 15 minutes, the third component (4-hydroxycoumarin) was introduced, promoting the formation of the advanced intermediate of m/z 368, evident

after 30 minutes during reaction monitoring. The Knoevenagel intermediate (m/z 308) was observed at very low abundance, signifying two key aspects: (i) successful avoidance of its formation exclusively by solvent selection, and (ii) when formed, immediate consumption, leading to the **DC** derivative. This is highlighted by the low intensity appearance of ions of m/z 470 and 492 (sodiated) related to the **DC** adduct. Similar outcomes were observed by switching the solvent from p-cymene to limonene (Fig. S4 and S5†) or other solvents with lower values of π^*. Changing the coumarin to the pyrone reagent (Fig. S6†) or to 4-aminocoumarin (Fig. S7†) yielded comparable results.

In our ongoing efforts to address this issue, we explored the substitution of the 4-hydroxy group in the coumarin reagent with urea (Scheme 7). This modification resulted in the formation of the 4-aminocoumarin derivative with yields exceeding 80%, along with a few minor byproducts. Among these byproducts, we isolated less than 5 mg of a guanidine derivative during a gram-scale synthesis. The guanidine-coumarin derivative was characterized using ESI-MS/MS and employed to monitor the reaction in the gas phase, with the goal of generating a **CPD** analogue structure similar to the original
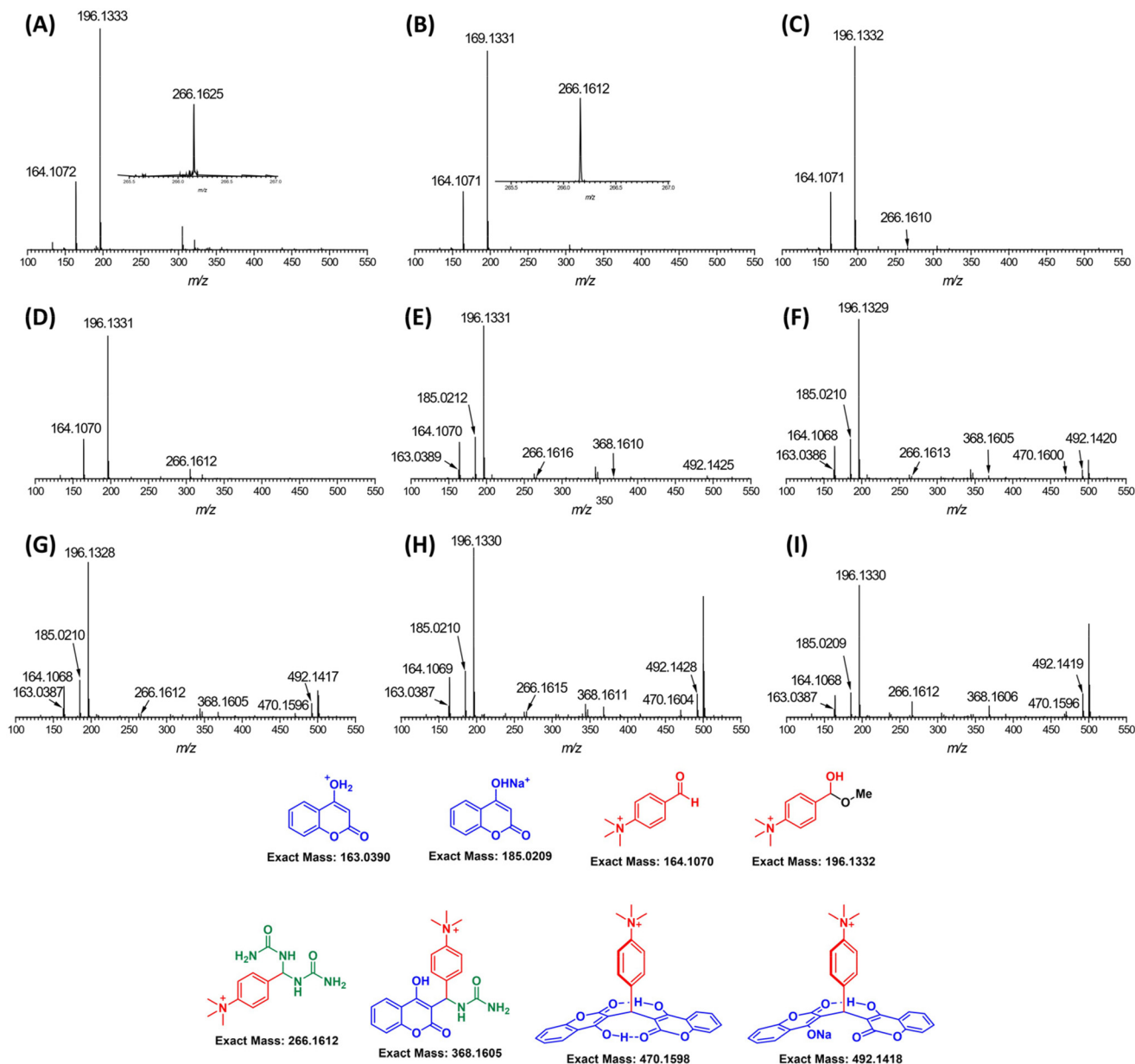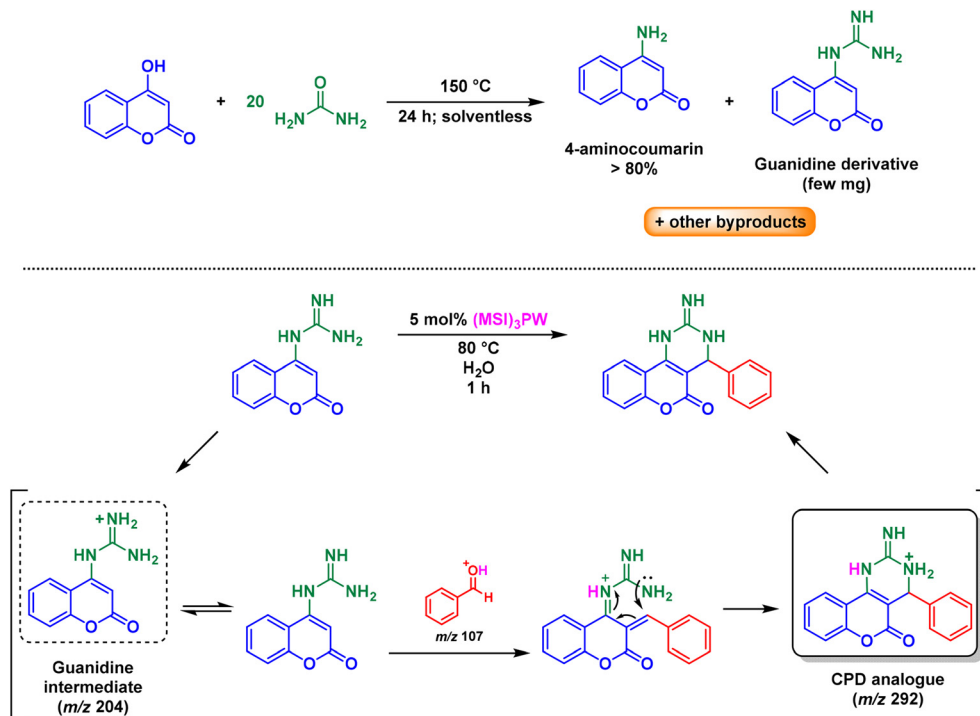
3638 | *Org. Biomol. Chem.*, 2024, **22**, 3630–3651

This journal is © The Royal Society of Chemistry 2024

Fig. 4 (Top) ESI(+)-MS monitoring using a charge-tagged aldehyde derivative in *p*-cymene aiming at the multicomponent synthesis of a **CPD** heterocycle. (A), (B), (C), (D), (E), (F), (G), (H), and (I) represent different reaction times, corresponding to 5, 10, 15, 20, 40, 60, 90, 120, and 240 min, respectively. (Bottom) Structures detected in the experiment and their calculated exact masses. Please note that the ion of *m/z* 196 is formed by the reversible methanol (the solvent in the ESI process) addition in the gas phase.

(Scheme 3) following an enamine-like reaction pathway. Application of the developed conditions led to the formation of an unprecedented guanidine-containing **CPD** analogue, which was monitored in the gas phase and characterized by MS/MS (Fig. 5). To the best of our knowledge, this is the first report of a **CPD**-like structure coherently characterized by its fragmentation pattern.

Building upon our prior efforts (Table 1), we have now chosen to synthesize a few **DC** derivatives (Scheme 8) to verify some biological properties. Although one of the tested ionic liquids yielded slightly better results (Table 1, entry 9), we

opted to conduct the reaction in water. This choice was motivated by the fact that the final **DC** products precipitate in this solvent, allowing for easy separation from the catalyst in the aqueous medium and facilitating the reuse of the water-soluble catalytic system. The catalytic system notably demonstrated sustained activity through at least three cycles with yields reaching up to 90%. This class of **DC** compounds is well-known for various biological activities,[172–174] including antibacterial properties,[175] inhibition of lipoxygenase enzymes,[176] anticoagulant effects,[177] antidiabetic effects,[178] and many others, as recently reviewed.[179]

This journal is © The Royal Society of Chemistry 2024

Org. Biomol. Chem., 2024, **22**, 3630–3651 | **3639**

Scheme 7 Synthesis of a guanidine derivative (top) and a **CPD** analogue (bottom).

All synthesized **DC** derivatives (Scheme 8) were obtained in good yields. Based on all the data obtained in this work, a plausible reaction mechanism could be proposed to explain the formation of **DC** compounds in the presence of the three components (urea or thiourea as contaminants) or simply by a pseudo-multicomponent transformation using two equivalents of coumarin, thereby also elucidating the unsuccessful formation of **CPDs** in these solvent-dependent equilibria (Scheme 9).

A brief discussion on the biological activities of the purported **CPD** derivatives should also be included. While we do not question the reported biological activities, particularly considering the well-established bioactivity of **DC** derivatives, a reassessment of the structure of these biologically active small molecules may be warranted. This reevaluation could shed light on biological responses such as antitubercular[92] and antiviral[97] activities claimed for the supposed **CPD** derivatives. CPDs activities against tumor cells have also been recently reviewed.[180]

Finally, we decided to assess the biological activities of **DC** derivatives synthesized using the pseudo-three-component approach, as well as those synthesized through the procedure aimed at evaluating the possible synthesis of **CPDs** (in the presence of urea/thiourea), to investigate any possible influence on the biological outcomes of an identified contaminant. The selected initial assay for this study was the etiolated wheat coleoptile bioassay, renowned for its rapidity in providing preliminary results within 24 h and its high sensitivity. Sensitivity was a crucial factor for our objective of assessing the influence of urea/thiourea as a contami-

nant. This technique is often suggested as the initial step in discovering potential new herbicides due to its high sensitivity,[181] with wheat coleoptile bioassays commonly used to identify herbicidal compounds. The use of pure **DC** derivatives (Fig. 6), synthesized without urea/thiourea, yielded expressive results. Comparable outcomes were observed when testing these **DC** derivatives contaminated with urea or thiourea (Fig. S8†).

In the conducted assays, it was observed that the majority of **DCs** significantly inhibited coleoptile growth, with **DC-03** standing out and exhibiting an IC_{50} lower than that of Logran® (commercially available – see Fig. S8†), which was used as a positive control. These results suggest a remarkable potential for the biological activity of these adducts, as most compounds demonstrated the inhibition of coleoptile growth. It is important to realize that this assay represents only a preliminary stage, making it essential to conduct additional studies to comprehensively evaluate the herbicidal activity of these products.

We also evaluated **DC-03** (both in its pure form and when contaminated) as an antitumoral agent. The aldehyde employed in the synthesis of this **DC** derivative, namely piperonal, is identical and bears substituents at specific positions that have been proven to be essential for the biological activity of a recognized Biginelli DHPM adduct known as Piperastrol (structure shown in Scheme 1).[182,183] The results obtained with contaminated **DC-03** (Fig. S9†) and pure **DC-03** (Fig. 7) were similar and comparable to those observed with Monastrol (Scheme 1), the DHPM used as the positive control in the experiment.
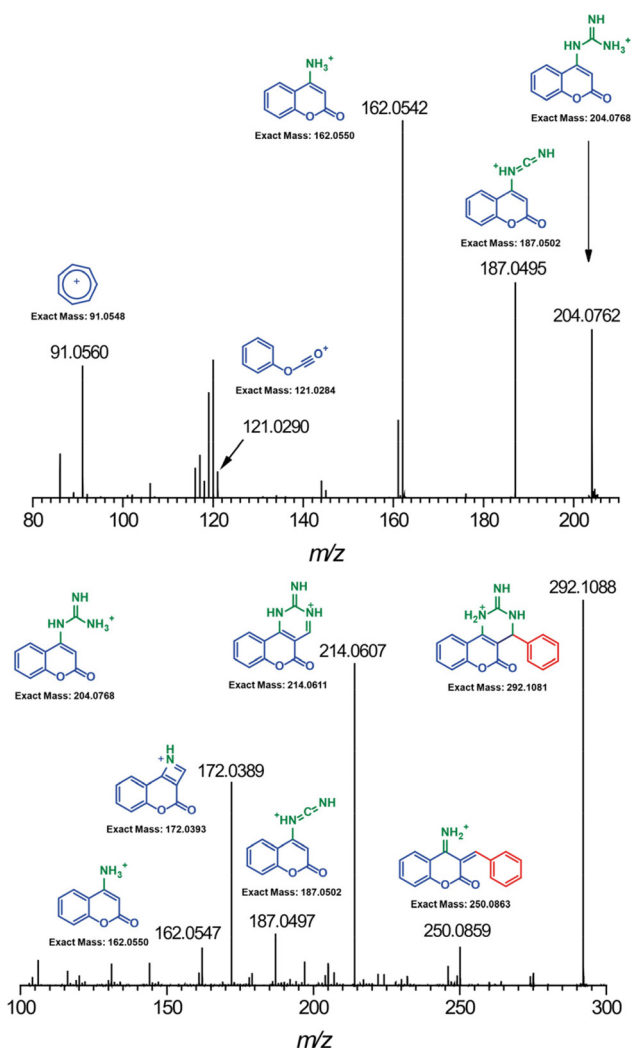
3640 | *Org. Biomol. Chem.*, 2024, **22**, 3630–3651

This journal is © The Royal Society of Chemistry 2024

Fig. 5 High resolution ESI(+)-MS/MS characterization of the guanidine-coumarin derivative (top) and of the guanidine-**CPD** analogue (bottom).

In the experiment, cell cycle arrest is observed in the monoastral mitotic spindle in the presence of both compounds (*i.e.*, **DC-03** and Monastrol). This result strongly suggests the inhibition of KSP/Eg5 kinesin activity *in vitro*, leading to the appearance of monoastral spindles in accordance with the literature.[44] This effect traps cells in the G2/M phase and ultimately leads to cell death. The negative control shows the normal spindle apparatus during the metaphase of mitosis in the tumoral MCF-7 cells. It is observed as a bipolar position of centrosomes, with microtubules emanating from opposite cell poles coupling opposing tension forces, aligning chromosomes at the cell equator, and preparing them for segregation to daughter cells. These features are inhibited by Monastrol and now, for the first time, described for a **DC** derivative.

One significant observation was the heightened density of microtubules in the monoastral mitotic spindle of cells treated exclusively with the **DC-03** small molecule. To better support these findings, docking studies were then conducted. Docking
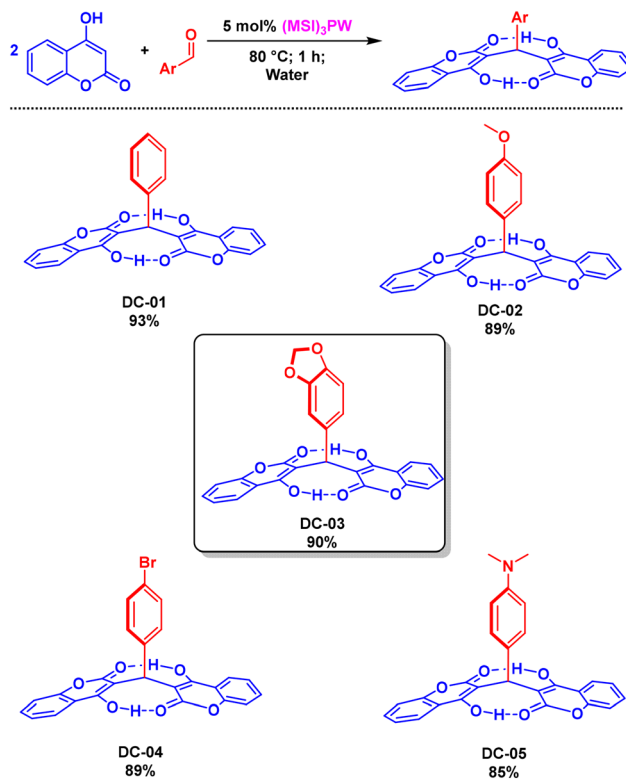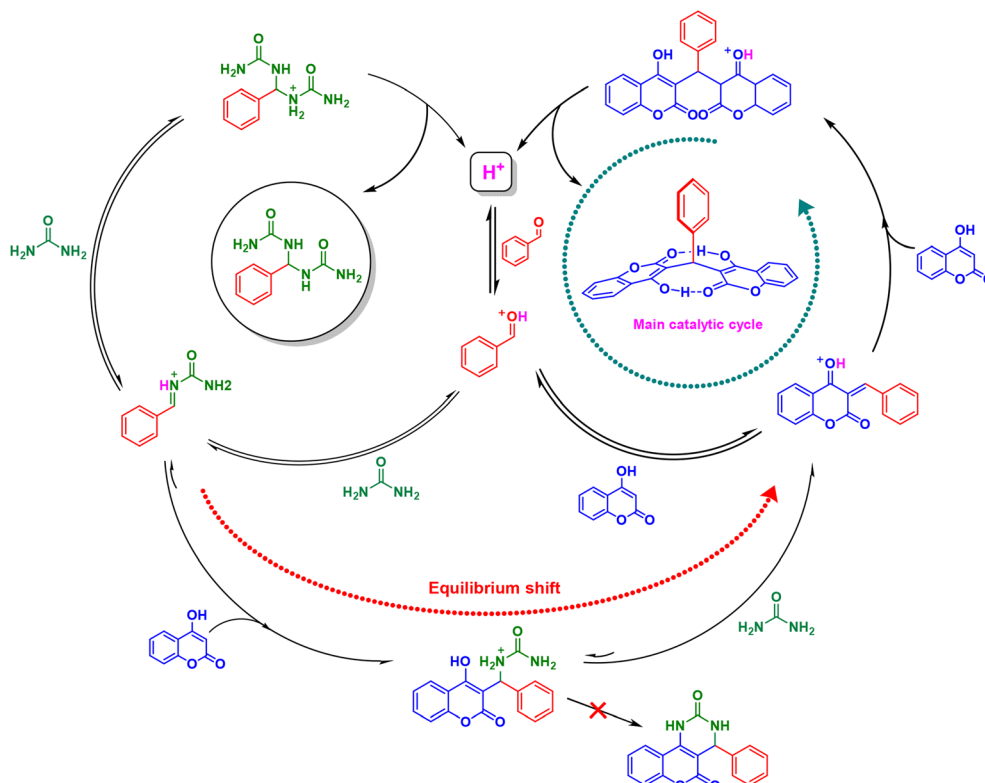

Scheme 8 Synthesis of certain **DC** derivatives under optimized conditions.

results using DOCK6[184,185] and the Monastrol-bound Eg5 (PDB 1Q0B)[186] indicated that both Monastrol and **DC-03** bind to Eg5 with similar poses (Fig. 8) and binding scores of −45.55 and −39.27 kcal mol^{-1}, respectively.

Due to its larger size, **DC-03** can penetrate deeper regions in the binding site, as confirmed by DOCK6's energy footprint (Fig. 9). While Monastrol forms stronger electrostatic interactions with the backbone of GLU118 and GLU116 (hydrogen bonds at 1.897 Å and 1.930 Å), **DC-03** establishes weaker electrostatic interactions with ARG119 and GLY117 (at 3.266 Å and 2.549 Å). **DC-03**, however, maintains stability in the binding site through hydrophobic interactions with additional residues such as PHE239 and ALA218. Fig. 9C illustrates that both inhibitors occupy identical binding sites, however, **DC-03** exhibits additional interactions compared to the positive control Monastrol.

Docking provides only a static snapshot of the system, and DOCK6's Continuous Energy scoring function does not account for conformational entropy and solvation/desolvation effects. Ligand stability in the binding site can be more accurately assessed through molecular dynamics (MD) simulations. Two unrestrained 10 ns MD simulations were then conducted using GROMACS 2020 to evaluate the stability of both ligands within the binding site by measuring the RMSD with respect to the initial production state. Each ligand was assigned GAFF2[187,188] parameters and AM1-BCC[189,190] partial charges using AmberTools22[191] Antechamber.[192] AmberTools' tleap

This journal is © The Royal Society of Chemistry 2024

Org. Biomol. Chem., 2024, **22**, 3630–3651 | **3641**

Scheme 9 Plausible catalytic cycles and equilibria observed under catalytic acidic conditions that explain the preferential formation of **DC** derivatives and the unsuccessful formation of **CPD** heterocycles. Note that these equilibria are solvent-dependent.
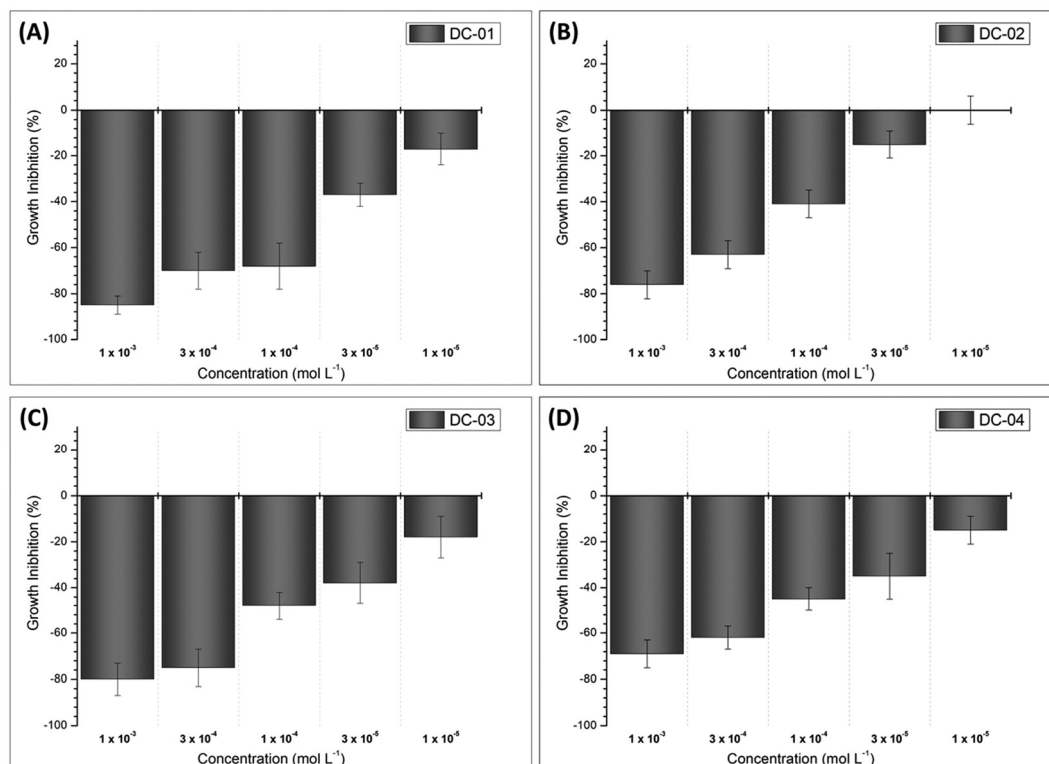

Fig. 6 Results of growth inhibition of coleoptile fragments for the treatments with selected **DC** derivatives.

3642 | Org. Biomol. Chem., 2024, **22**, 3630–3651

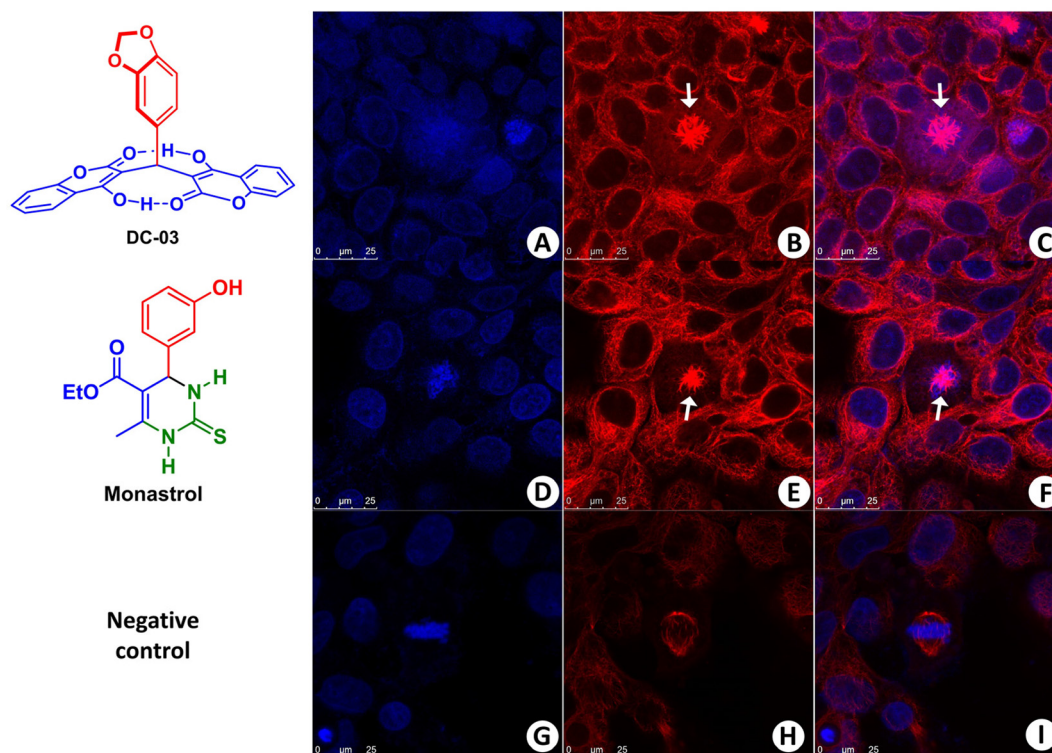This journal is © The Royal Society of Chemistry 2024

Fig. 7 Cellular division (mitosis) inhibition of MCF-7 cells type by **DC-03** (top) and by Monastrol, the positive control (center) and the negative control (bottom). (A), (D) and (G) Nuclei stained with the commercially available DAPI (blue emitter). (B), (E) and (H) Anti-α-Tubulin monoclonal antibody (commercially available red emitter). (C), (F) and (I) Merged images from (A), (B), (D), (E) and (G), (H), respectively. Note that **DC-03** induced monoastral spindles in mitotic cells, similar to the positive control.
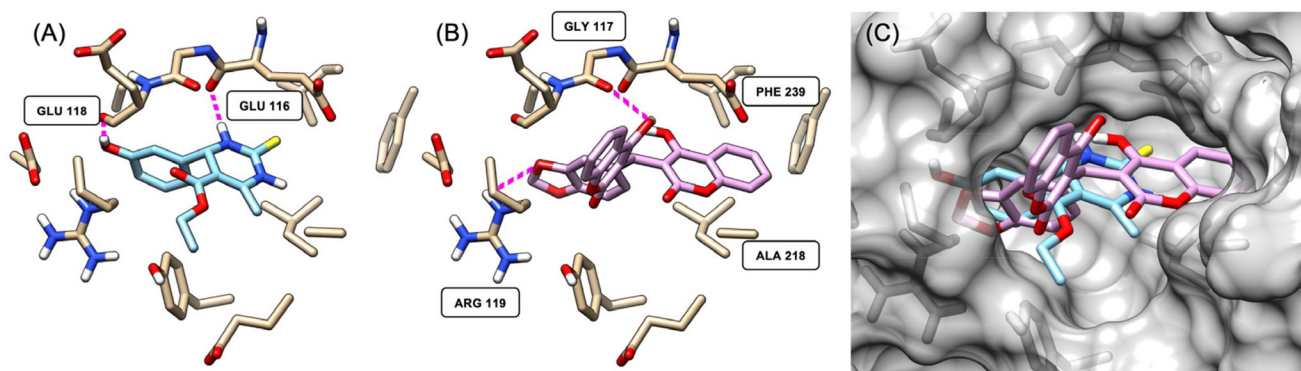

Fig. 8 Docked poses of Monastrol (A) and **DC-03** (B) in Eg5 (PDB 1Q0B). CE represents DOCK6's Continuous Energy score. Only relevant portions of the residues and their side chains are displayed and hydrogen atoms bonded to carbon atoms are hidden. Magenta dashed lines indicate the most significant electrostatic interactions between each ligand and the binding site. Panel (B) illustrates that **DC-03** penetrates deeper into Eg5's binding pocket. (C) Overlay of Monastrol and **DC-03** binding sites on Eg5.

was utilized to assign ff14SB parameters,[193] protonate the protein, generate the receptor–ligand complex, and solvate the system with TIP3P water.[194] The resulting files were converted to the GROMACS format using ParmEd.[195] Production runs followed one minimization and four equilibration stages (see details in the ESI†) and were conducted at 298 K and 1 bar using a Langevin integrator and the Parrinello–Rahman baro-stat to ensure proper sampling in the NPT ensemble. RMSD analysis of the MD trajectory revealed that both Monastrol and **DC-03** maintain their poses in the binding site throughout the 10 ns production run (Fig. 10). Backbone RMSDs also suggest that neither ligand induces significant structural changes in Eg5's backbone, supporting the hypothesis that **DC-03** and Monastrol may act similarly.
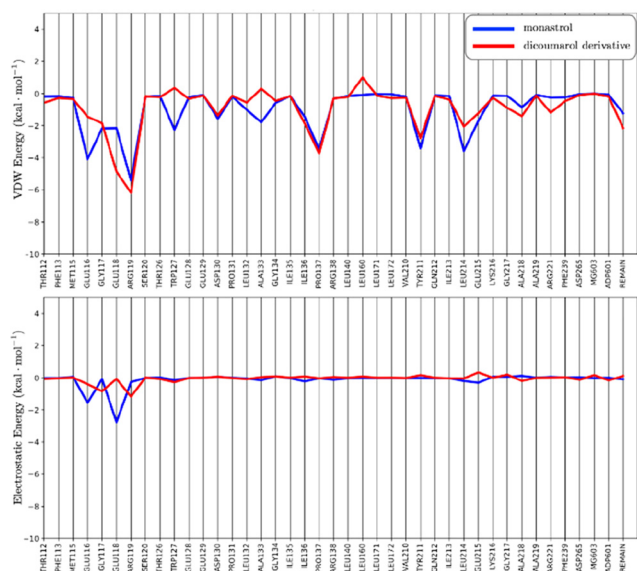
This journal is © The Royal Society of Chemistry 2024

Org. Biomol. Chem., 2024, **22**, 3630–3651 | **3643**

Fig. 9 Energy footprint of the interaction between Monastrol and **DC-03** with the binding site (blue and red, respectively). Each vertical line corresponds to a residue in the binding pocket, and the point where it intersects the colored curve represents its energy. The upper plot displays van der Waals (VDW) energy components, while the lower plot shows electrostatic energies. Monastrol and **DC-03** exhibit similar VDW energy footprints and share crucial electrostatic interactions in adjacent residues (GLU116, GLY117, GLU118, ARG119).
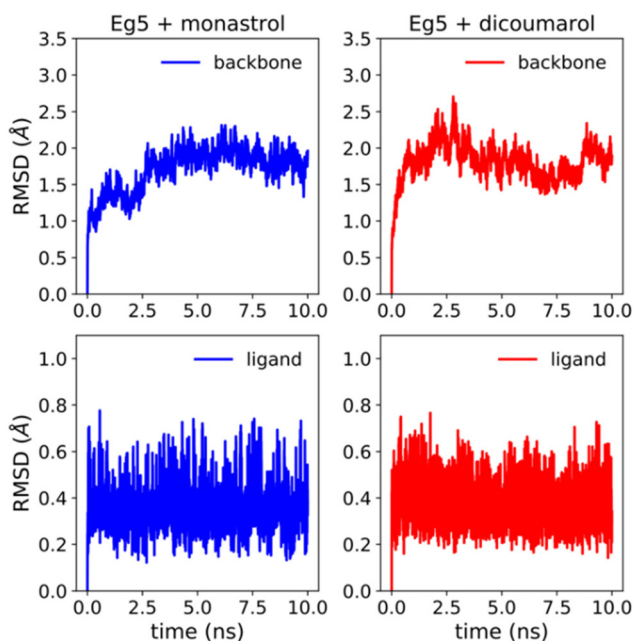

Fig. 10 RMSD analysis of Monastrol and dicoumarol derivative **DC-03** in Eg5. The average backbone RMSD was 1.709 Å for Eg5 + Monastrol and 1.811 Å for Eg5 + **DC-03**. The average RMSDs for the ligands in the binding pocket were, respectively, 0.351 Å and 0.383 Å.

Conclusions

In summary, we applied a solvent effect model based on Kamlet–Taft descriptors to assess various Biginelli-like reac-

tions. The initial, seemingly contradictory results, however, led us in a different direction, highlighting a crucial issue. A comprehensive examination of literature reports, along with their spectroscopic and spectrometric data, and the appropriate application of Kamlet–Taft parameters allowed us to identify structural misassignments in a few Biginelli-like reactions. In these cases, dicoumarol derivatives were likely forming instead of the expected MCR adducts, and the presence of urea (or thiourea) contaminants resulted in lower melting points. Our attempts to reproduce the literature conditions also failed in the cases indicated herein.

The use of ESI-MS(/MS) to monitor the reaction, with and without charge-tagged reagents, prompted further inquiry into the asserted MCRs and the proposed mechanisms for their formation. The data we obtained supported our claims and indicated the misassignment of several MCRs adducts. All efforts to obtain **CPD** adducts only yielded **DC** derivatives contaminated with a third component from the reaction (*i.e.*, urea). An analogue of a **CPD** structure was obtained in very low yields, allowing only for its MS/MS structural characterization, but it also highlighted the inaccuracy of the literature. A major conclusion is that **CPD** synthesis remains a synthetic challenge, and this structure needs to be obtained through different methodologies and synthetic sequences, as no MCR condition described so far has allowed its production. All analyses calculations shed light on the reaction mechanism and the reasons for the synthetic failure of the methodologies described so far.

Biological investigations with pure and "contaminated" **DC** derivatives indicated that the presence of urea or thiourea did not significantly affect the biological response in the investigated bioassays. A new mechanism of cellular action was revealed for a dicoumarol derivative, and the initial data strongly suggested a similarity between the known DHPM called Monastrol and **DC-03** as Eg5 inhibitors, both of which induce a monoastral mitotic spindle, thus preventing the normal mitotic process. Docking studies and RMSD supported this hypothesis. Further experiments are necessary to delve deeper into this new class of Eg5 inhibitors, and they will be disclosed in due course.

Finally, we recommend revisions, possibly the publication of a corrigendum, for those articles with incorrect structural assignments. These syntheses are currently being "reproduced" without critical evaluation and proper characterization. These derivatives are being described as bioactive compounds with different biological responses, necessitating a structural correction and recalculation of dose-responses based on the actual structure of the bioactive compounds.

Experimental section

General methods

All purchased chemicals were used as received without further purification unless indicated. All solvents employed were of commercial grade, and when necessary, they underwent distil-

3644 | *Org. Biomol. Chem.*, 2024, **22**, 3630–3651

This journal is © The Royal Society of Chemistry 2024

lation. All reactions were carried out in a temperature-controlled oil bath. ^{1}H (600 MHz) and ^{13}C{^{1}H} (150 MHz) NMR spectra were recorded in CDCl$_3$ or DMSO-d_6 solution with tetramethylsilane (TMS) used as the internal standard. Multiplicities were denoted as follows: s (singlet), d (doublet), t (triplet), td (triple doublet), q (quartet), and m (multiplet). Chemical shifts are expressed in δ ppm and coupling constants (J) are provided in Hz. Electrospray ionization (tandem) mass spectrometry analyses were conducted on an instrument, equipped with an ESI source, and with the accelerator TOF analyzer. Fourier-transform infrared (FTIR) spectra were obtained using a Fourier Transform Infrared Spectrometer. The samples were prepared in KBr pellets. Melting points were determined using an apparatus equipped with an oil bath, and the heating rate for the analyses was set at 1 °C min^{-1}.

General procedure for the synthesis attempts of 4-phenyl-3,4-dihydro-2*H*-chromeno[4,3-*d*]pyrimidine-2,5(1*H*)-dione (CPD-01) based on previous reports (see Scheme 2 for references)

Attempt 1 (enantioselective attempt): equimolar ratios of 4-hydroxycoumarin (1 mmol, 0.16 g), benzaldehyde (1 mmol, 0.11 g), and urea (1 mmol, 0.06 g) were mixed in a round-bottom flask with 10 mol% L-proline as the chiral catalyst (11 mg) and 1 mL of water. The mixture was microwave-irradiated at 70 °C for 10 min. The resulting solid was filtered, washed with EtOH/H$_2$O (1 : 1, v/v), dried, and recrystallized in ethanol, yielding 59% (250 mg) of **DC-01**.

Attempt 2: in a round-bottom flask, 4-hydroxycoumarin (1 mmol, 0.16 g), benzaldehyde (1 mmol, 0.11 g), and urea (1 mmol, 0.06 g) were combined with 10 mol% sodium lauryl sulfate (30 mg) and 5 mL of water. The mixture was stirred for 5 h at 25 °C. The precipitate was filtered, washed with EtOH/H$_2$O (1 : 1, v/v), dried, and recrystallized in ethanol, yielding 34% (144 mg) of **DC-01**.

Attempt 3: 4-hydroxycoumarin (1 mmol, 0.16 g), benzaldehyde (1 mmol, 0.11 g), urea (1 mmol, 0.06 g), 20 mol% of SLS (60 mg), 2 drops of acetic acid, and 10 mL of water were reacted in a Schlenk flask at 100 °C for 6 h. The solid was filtered, washed with hot water (30 mL, 80 °C) and 5 mL of ethanol, dried, and recrystallized in ethanol, yielding 51% (216 mg) of **DC-01**.

Attempt 4 (this work): in a Schlenk tube, 1 mmol of 4-hydroxycoumarin (0.16 g), benzaldehyde (0.11 g), urea (0.06 g), and 5 mol% of the superacid catalyst (MSI)$_3$PW (0.17 g) were reacted at 80 °C for 1 h. 1 mL of the following solvents were also tested: water, ethanol, methanol, ethyl acetate, *t*-butanol, acetonitrile, hexane, THF, dioxane, triethylamine, cyclohexane, octanol, 2,2,2-trifluoroethan-1-ol, acetone, chloroform, BMI·PF$_6$, BMI·BF$_4$, BMI·NTf$_2$, dichloromethane, toluene, *p*-cymene, and limonene. After completion, the precipitate was filtered, washed with hot water and ethanol, dried, and recrystallized in ethanol. For all cases, **DC-01** was obtained (see Table 1).

Attempt 5 (this work): in a round-bottom flask, 0.05 mmol of urea (0.03 g), 0.05 mmol of 4-formyl-*N*,*N*,*N*-trimethyl-

benzenaminium (charge-tagged aldehyde), and 5 mL of solvent (*p*-cymene or limonene) were stirred for 20 min at 80 °C. Then, 0.05 mmol of 4-hydroxycoumarin was added, and the mixture was kept at the same temperature for up to 24 h. This procedure was repeated, but with temperature raised from 80 to 140 °C. The reactions were monitored by HRMS and only **DC-01** was observed.

Attempt 6 (this work): in a sealed Schlenk tube, 1 mL of water or *p*-cymene, 1 mmol of 4-hydroxycoumarin (0.16 g), benzaldehyde (0.11 g), urea (0.06 g), and 10 mol% *t*-BuOK (0.12 g) were mixed. The reaction was maintained at 140 °C for 2 h. The reaction mixture was analyzed by HRMS and only **DC-01** was observed.

General procedure for the synthesis attempts of 7-phenyl-6*H*,7*H*-benzo[4,5]thiazolo[3,2-*a*]chromeno[4,3-*d*]pyrimidin-6-one (TPC-01)

Attempt 1: in a round-bottom flask, 1 mmol each of 4-hydroxycoumarin (0.16 g), benzaldehyde (0.11 g), and benzothiazol-2-amine (0.15 g) were combined with 10 mol% sodium lauryl sulfate as the catalyst (0.03 g) in 10 mL of water. The mixture was stirred for 5 h at 25 °C. After the reaction, the precipitate was filtered, dried, and recrystallized in ethanol. Only **DC-01** (43%, 182 mg) was observed.

Attempt 2: in a round-bottom flask, 1 mmol of each reagent *i.e.*, 4-hydroxycoumarin (0.16 g), benzaldehyde (0.11 g), and benzothiazol-2-amine (0.15 g) were combined with 5 mol% (MSI)$_3$PW as the catalyst (0.17 g) in 5 mL of ethanol. The mixture was stirred for 2 h at 50 °C. The precipitate was then filtered, washed with hot water and ethanol, and recrystallized in ethanol. Only **DC-01** (39%, 165 mg) was observed.

General procedure for the synthesis of 2-amino-5-oxo-4-phenyl-4*H*,5*H*-pyrano[3,2-*c*]chromene-3-carbonitrile (APC-01)

Method A: in a round-bottom flask, 5 mmol of each reagent *i.e.*, benzaldehyde (0.53 g), malononitrile (0.33 g), and urea (38 mg) as the catalyst were combined with 5 mL of a 1 : 1 (v/v) EtOH/H$_2$O solution. The mixture was stirred at 30 °C for 20 min, and then 5 mmol of 4-hydroxycoumarin (0.81 g) was added. The reaction proceeded at 30 °C for 6 h. **DC-01** (65%, 1.38 g) and **ACP-01** (35%, 0.55 g) were isolated.

Method B: in a sealed Schlenk tube, 1 mmol of benzaldehyde (0.11 g), malononitrile (0.07 g), and 4-hydroxycoumarin (0.16 g) were combined with 5 mol% *t*-BuOK as the catalyst (16 mg) and 1 mL of ethanol. The mixture was heated to 80 °C for 30 min. The resulting solid precipitate was filtered, washed with EtOH/H$_2$O solution, and recrystallized in ethanol. **ACP-01** (80%, 253 mg) was isolated.

Yield 1.24 g (78%, Method A) and 0.24 g (49%, Method B); white solid; m.p. 257–259 °C; ^{1}H NMR (600 MHz, DMSO-d_6) δ ppm 7.91 (dd, J = 8.0, 1.5 Hz, 1H), 7.70 (ddd, J = 8.4, 7.4 Hz, 1.6, 1H), 7.48 (ddd, J = 7.9, 7.5, 1.0 Hz, 1H), 7.45 (dd, J = 8.3, 0.6 Hz, 1H), 7.40 (s, 2H), 7.31 (tt, J = 3.5, 1.7 Hz, 2H), 7.24 (m, 4H), 4.44 (s, 1H); ^{13}C{^{1}H} NMR (150 MHz, DMSO-d_6) δ ppm 159.6, 158.3, 153.5, 152.2, 143.4, 133.0, 128.6, 127.7, 127.2, 124.7, 122.5, 119.3, 116.6, 113.0, 104.4, 58.0, 37.0; FTIR (cm^{-1})

3378, 3284, 3180, 2198, 1708, 1673, 1608, 1380, 1058; HRMS (ESI) m/z [M + H]$^+$ calcd for [C$_{27}$H$_{21}$NO + H]$^+$, 317.0921, found, 317.0923.

General procedure for the synthesis of 10,10-dimethyl-7-phenyl-7,9,10,11-tetrahydro-6H,8H-chromeno[4,3-b]chromene-6,8-dione (TCC)

In a round-bottom flask, the following components were combined: (MSI)$_3$PW (0.81 g, 5 mol%), 4-hydroxycoumarin (0.82 g, 5 mmol), 5,5-dimethyl-1,3-cyclohexanedione (0.70 g, 5 mmol), benzaldehyde (0.50 g, 5 mmol), and water (10 mL). The resulting mixture underwent heating at 80 °C and continuous stirring at this temperature for 2 h. Subsequently, the reaction mixture was allowed to cool to room temperature, followed by filtration and thorough washing with hot water to isolate the catalyst. The resulting crude product was subjected to purification through recrystallization using an EtOH/CH$_2$Cl$_2$ solvent mixture (1 : 4, v/v).

Yield 1.23 g (63%), white solid; mp 222–224 °C; ^{1}H NMR (600 MHz, CDCl$_3$) δ ppm 7.81 (dd, J = 7.9, 1.5 Hz, 1H), 7.50 (ddd, J = 8.7, 7.5, 1.5 Hz, 1H), 7.33–7.24 (m, 4H), 7.29–7.25 (m, 2H), 7.20–7.17 (m, 1H), 4.90 (s, 1H), 2.63 (q, J = 17.6 Hz, 2H), 2.23 (q, J = 16.2 Hz, 2H), 1.11 (s, 3H), 1.03 (s, 3H); ^{13}C{^{1}H} NMR (150 MHz) δ ppm 196.1, 162.1, 160.7, 154.0, 152.7, 142.6, 132.3, 128.7, 128.4, 127.2, 124.4, 122.6, 117.0, 115.3, 113.8, 106.9, 50.8, 40.9, 33.5, 32.5, 29.3, 27.7; FTIR (cm^{-1}) 3425, 3064, 2956, 2869, 1714, 1658, 1365, 1192, 1170, 1055, 761. HRMS (ESI) m/z [M + H]$^+$ calcd for [C$_{24}$H$_{20}$O$_4$ + H]$^+$, 373.1434; found, 373.1438.

General procedure for the synthesis of dicoumarol derivatives (DCs)

In a sealed Schlenk tube, 2 mmol of 4-hydroxycoumarin (0.33 g), 1 mmol of respective aldehyde, 5 mol% of (MSI)$_3$PW catalyst (170 mg), and 1 mL of water as a solvent were added, and the mixture was heated to 80 °C for 1 h. Upon completion of the reaction, the precipitate was filtered and washed with a hot solution of EtOH/H$_2$O (1 : 1, v/v). Subsequently, when necessary, the desired product was recrystallized in ethanol to obtain the pure product. For a multigram synthesis, the same procedure is applied but using 10 mmol of 4-hydroxycoumarin (1.60 g), 10 mmol of benzaldehyde (1.06 g), 5 mol% of (MSI)$_3$PW catalyst (1.74 g), and 5 mL of water.

3,3′-(Phenylmethylene)bis(4-hydroxy-2H-chromen-2-one) (DC-01)

Yield 403 mg (88%) and 2.5 g (93%, in the multigram synthesis); White solid; m.p. 230–231 °C; ^{1}H NMR (600 MHz, DMSO-d_6) δ ppm 7.92 (d, J = 7.9 Hz, 2H), 7.60 (t, J = 8.3 Hz, 2H), 7.38 (d, J = 8.3 Hz, 2H), 7.33 (t, J = 7.9 Hz, 2H), 7.24 (t, J = 7.9 Hz, 2H), 7.17–7.14 (m, 3H); ^{13}C{^{1}H} NMR (150 MHz, DMSO-d_6) δ ppm 165.1, 164.9, 152.2, 139.7, 132.0, 128.1, 126.7, 125.7, 123.9, 123.8, 118.0, 116.0, 104.2, 36.0; FTIR (cm^{-1}) 3446, 3068, 2736, 2615, 1660, 1616, 1604, 1567, 1495, 1450, 1346, 1299, 1182, 1093, 759; HRMS (ESI) m/z [M + H]$^+$ calcd for [C$_{25}$H$_{16}$O$_6$ + H]$^+$, 413.1020, found, 413.1019.

3,3′-((4-Methoxyphenyl)methylene)bis(4-hydroxy-2H-chromen-2-one) (DC-02)

Yield 267 mg (89%); white solid; m.p. 247–248 °C. ^{1}H NMR (600 MHz, DMSO-d_6) δ ppm 7.92 (d, J = 7.9 Hz, 2H), 7.60 (t, J = 7.9 Hz, 2H), 7.39 (dd, J = 8.2, 2.1 Hz, 2H), 7.34 (t, J = 7.9 Hz, 2H), 7.07 (d, J = 6.6 Hz, 2H), 6.80 (d, J = 8.6 Hz, 2H), 6.31 (s, 1H), 3.70 (s, 3H). ^{13}C{^{1}H} NMR (150 MHz, DMSO-d_6) δ ppm 164.9, 157.4, 152.2, 132.0, 131.2, 127.8, 123.9, 117.7, 116.0, 113.6, 104.5, 55.0, 35.2. FTIR (cm^{-1}) 3448, 3068, 3002, 2937, 2836, 2732, 2616, 1668, 1617, 1604, 1560, 1510, 1454, 1353, 1309, 1257, 1178, 1093, 767 HRMS (ESI) m/z [M + H]$^+$ calcd for [C$_{26}$H$_{18}$O$_7$ + H]$^+$ 443.1125 found, 443.1122.

3,3′-(Benzo[d][1,3]dioxol-5-ylmethylene)bis(4-hydroxy-2H-chromen-2-one) (DC-03)

Yield 232 mg (90%); pale yellow solid; m.p. 258–260 °C; ^{1}H NMR (600 MHz, DMSO-d_6) δ ppm 7.92 (d, J = 7.9, 1.5 Hz, 2H), 7.59 (td, J = 8.7, 3.2 Hz, 2H), 7.36 (d, J = 8.3, 2H), 7.32 (t, 8.3, 2H), 6.76 (d, J = 8.2 Hz, 1H), 6.71 (s, 1H), 6.62 (dt, J = 8.0, 1.5 Hz, 1H), 6.26 (s, 1H), 5.94 (s, 3H); ^{13}C{^{1}H} NMR (150 MHz, DMSO-d_6) δ ppm 165.2, 164.8, 152.3, 147.4, 145.3, 133.7, 132.0, 123.9, 123.8, 119.5, 117.9, 116.0, 107.8, 107.6, 104.4, 100.7, 35.8; FTIR (cm^{-1}) 3448, 3081, 2898, 2736, 2615, 1662, 1616, 1602, 1567, 1488, 1436, 1344, 1309, 1236, 1097, 1039, 763; HRMS (ESI) m/z [M + H]$^+$ calcd for [C$_{26}$H$_{16}$O$_8$ + H]$^+$, 457.0918, found, 457.0916.

3,3′-((4-Bromophenyl)methylene)bis(4-hydroxy-2H-chromen-2-one) (DC-04)

Yield 346 mg (89%); white solid; m.p. 267–268 °C; ^{1}H NMR (600 MHz, DMSO-d_6) δ ppm 7.89 (dd, J = 7.9, 1.4 Hz, 2H), 7.58 (t, J = 8.0 Hz, 2H), 7.38 (d, J = 9 Hz, 2H), 7.35 (d, J = 8.0 Hz, 2H), 7.31 (t, J = 7.9 Hz, 2H), 7.11 (d, J = 8.6 Hz, 2H), 6.29 (s, 1H); ^{13}C{^{1}H} NMR (150 MHz, DMSO-d_6) δ ppm 165.8, 164.7, 152.3, 140.1, 131.9, 130.8, 129.2, 124.0, 123.7, 118.5, 118.4, 116.0, 103.8, 35.8; FTIR (cm^{-1}) 3428, 3070, 2728, 2609, 1668, 1617, 1604, 1560, 1488, 1351, 1307, 1093, 765. HRMS (ESI) m/z [M + H]$^+$ calcd for [C$_{25}$H$_{15}$BrO$_6$ + H]$^+$, 491.0125, found, 491.0120.

3,3′-((4-(Dimethylamino)phenyl)methylene)bis(4-hydroxy-2H-chromen-2-one) (DC-05).

Yield 235 mg (85%); pink solid; m.p. 200–201 °C; ^{1}H NMR (600 MHz, DMSO-d_6) δ ppm 7.83 (dd, J = 7.9, 1.3 Hz, 2H), 7.52 (t, J = 7.9 Hz, 2H), 7.44 (d, J = 7.9 Hz, 2H), 7.31–7.23 (m, 7H), 6.30 (s, 1H), 3.15 (s, 6H); ^{13}C{^{1}H} NMR (150 MHz, DMSO-d_6) δ ppm 167.5, 164.4, 152.5, 131.2, 128.2, 124.1, 123.0, 119.6, 115.6, 103.0, 45.6, 36.0; FTIR (cm^{-1}) 3434, 3045, 2917, 2792, 1673, 1606, 1540, 1400, 1351, 1043, 755; HRMS (ESI) m/z [M + H]$^+$ calcd for [C$_{27}$H$_{21}$NO$_6$ + H]$^+$, 456.1442, found, 456.1439.

Bioimaging. The breast cancer cell line (MCF-7) was maintained following the recommendations of the American Type Culture Collection (ATCC). **DC-03** and Monastrol were diluted to 100 μM in Dulbecco's Modified Eagle's medium (DMEM) supplemented with 0.1% dimethyl sulfoxide and 10% fetal calf serum. 7 × 10^4 cells were seeded on 13 mm cover slips inside a 24-well plate for 48 h to reach 75% confluence. The samples

3646 | *Org. Biomol. Chem.,* 2024, **22**, 3630–3651

This journal is © The Royal Society of Chemistry 2024

were divided into three groups and incubated under the following conditions for 48 h: (A) negative control incubated with only culture medium plus 0.1% DMSO; (B) positive control incubated with Monastrol at 100 μM; and (C) incubated with **DC-03** at 100 μM. After 48 h, the samples were washed three times with warm PBS (37 °C), pH 7.4, and subjected to fixation procedures in 3.7% formaldehyde for 30 minutes at room temperature.

Immunofluorescence assay. Fixed samples were permeabilized in 0.1% Triton X-100 for 20 min and then incubated in a blocking solution (PBS, pH 7.4, 1% skimmed milk, 2.5% bovine serum albumin, 8% fetal calf serum) for additional 20 min. Subsequently, the samples were incubated with a primary antibody (anti-α-tubulin) produced in mouse for 16 h at 4 °C. After three washes with PBS, pH 7.4, at room temperature, the samples were incubated for 1 h at 37 °C with a secondary antibody, Alexa Fluor 594 anti-mouse (5 μg mL^{-1}), in the dark. Following three additional washes in PBS, pH 7.4, the samples were incubated for 5 min with DAPI (300 nM) to stain the cell nucleus. After three more washes in PBS, pH 7.4, the samples were mounted on glass slides using ProLong Gold Antifade agent and analyzed using a confocal laser scanning microscope.

Computational methods

Docking simulations details. Preparation step: 1Q0B structure was downloaded from RCSB Protein Data Bank using UCSF Chimera. The asymmetric unit consisted of a dimer bound to two Monastrol molecules and two ADP molecules. One monomer and excess crystalized water molecules were deleted, remaining a monomer, ADP complexed to Mg^{2+} and adjacent water molecules, and Monastrol. The crystal structure was initially relaxed using energy minimization and a short heavy-atom restricted NVT MD run at 298 K in GROMACS 2020 to ensure that steric hindrance between the ligands and the protein was minimized. The protein was parameterized with ff14SB and the ligands with GAFF2 with AM1-BCC charges.

Docking step. After ensuring that any steric hindrance was minimized, Monastrol was removed from the binding pocket and the surface of the protein was generated using DMS[196] with a 1.4 Å radius probe atom. Docking spheres were generated inside the binding pocket with DOCK's sphgen.[197] 1Q0B energy grids were generated using the program grid.[198] Each grid point had a coulombic energy term using a distance-dependent dielectric of 4r and a 6–9 Lennard Jones term. Dicoumarol was docked using DOCK6's Grid scoring function and the best binding pose was minimized and rescored using DOCK6's Continuous Energy (CE) scoring function. The original ligand, Monastrol, was minimized and scored with CE. Energy footprints were generated for minimized structures in the binding site.

Molecular dynamics step. Monastrol original pose and **DC-03** best scoring pose were prepared for MD in a similar fashion to the pre-docking preparation step. The receptor was assigned ff14SB parameters and the ligands were assigned GAFF2 parameters and AM1-BCC charges. Tleap was used to solvate and neutralize each receptor–ligand complex. The 10 ns production step was preceded by one minimization and four equilibration steps. Energy minimization was run with a steepest descent algorithm with an energy tolerance of 10 kJ mol^{-1} and step sizes of 0.01 kJ mol^{-1}. The first equilibration step (NVT) was a 100 ps simulation with a Langevin integrator set to generate configurations at 298 K with a step size of 2 fs. All non-solvent heavy atoms were kept in place by a 1000 kJ mol^{-1} position restraint. The second equilibration step (NPT_1) was set in the same way as the NVT equilibration step with the addition of a Berendsen barostat to bring the density and the pressure of the simulation box to near-equilibrium conditions at 1 bar. The third equilibration step (NPT_2) used the Parrinello-Rahman barostat instead to ensure sampling is adequate in the isothermal–isobaric ensemble. The fourth equilibration step (NPT_3) differed from NPT_2 by the restraints in the receptor. In NPT_3, only the backbone was restrained, and side chains were allowed to move freely. The production stage (PROD) was run with a completely unrestrained system at 298 K and 1 bar using the same integrator and barostat as the previous step. Excepting the minimization step, bonds to hydrogen were constrained using GROMACS' implementation of LINCS. van der Waals interactions were neglected beyond a cutoff of 12 Å with a switch at 10 Å, and electrostatic interactions were calculated using the Particle Mesh Ewald (PME) method of order 4 with a real-space cutoff of 12 Å and grid spacing of 1.6 Å. Periodic boundary conditions were applied.

Author contributions

All authors had important contributions to this work.

Conflicts of interest

The authors declare no competing financial interest.

Acknowledgements

References

1 B. A. D. Neto, M. N. Eberlin and J. Sherwood, *Eur. J. Org. Chem.*, 2022, e202200172.
2 B. A. D. Neto, R. O. Rocha and M. O. Rodrigues, *Molecules*, 2022, **27**, 132.
3 C. J. Clarke, W. C. Tu, O. Levers, A. Brohl and J. P. Hallett, *Chem. Rev.*, 2018, **118**, 747–800.
4 J. Sherwood, J. H. Clark, I. J. S. Fairlamb and J. M. Slattery, *Green Chem.*, 2019, **21**, 2164–2213.
5 Y. Marcus, *Chem. Soc. Rev.*, 1993, **22**, 409–416.

This journal is © The Royal Society of Chemistry 2024

Org. Biomol. Chem., 2024, **22**, 3630–3651 | **3647**

6 M. J. Albaladejo, F. Alonso and M. J. Gonzalez-Soria, *ACS Catal.*, 2015, **5**, 3446–3456.

7 R. Ramozzi and K. Morokuma, *J. Org. Chem.*, 2015, **80**, 5652–5657.

8 S. Santra and P. R. Andreana, *Org. Lett.*, 2007, **9**, 5035–5038.

9 E. F. Freitas, R. Y. Souza, S. T. A. Passos, J. A. Dias, S. C. L. Dias and B. A. D. Neto, *RSC Adv.*, 2019, **9**, 27125–27135.

10 K. Guo, M. J. Thompson and B. N. Chen, *J. Org. Chem.*, 2009, **74**, 6999–7006.

11 G. A. Price, A. K. Brisdon, K. R. Flower, R. G. Pritchard and P. Quayle, *Tetrahedron Lett.*, 2014, **55**, 151–154.

12 J. H. Clark, D. J. Macquarrie and J. Sherwood, *Chem. – Eur. J.*, 2013, **19**, 5174–5182.

13 H. G. O. Alvim, T. B. Lima, A. L. de Oliveira, H. C. B. de Oliveira, F. M. Silva, F. C. Gozzo, R. Y. Souza, W. A. da Silva and B. A. D. Neto, *J. Org. Chem.*, 2014, **79**, 3383–3397.

14 G. H. C. Oliveira, L. M. Ramos, R. K. C. de Paiva, S. T. A. Passos, M. M. Simoes, F. Machado, J. R. Correa and B. A. D. Neto, *Org. Biomol. Chem.*, 2021, **19**, 1514–1531.

15 P. Noppawan, S. Sangon, N. Supanchaiyamat and A. J. Hunt, *Green Chem.*, 2021, **23**, 5766–5774.

16 M. H. R. Carvalho, J. P. R. S. Ribeiro, P. P. De Castro, S. T. A. Passos, B. A. D. Neto, H. F. Dos Santos and G. W. Amarante, *J. Org. Chem.*, 2022, **87**, 11007–11020.

17 R. C. Cioc, E. Ruijter and R. V. A. Orru, *Green Chem.*, 2014, **16**, 2958–2975.

18 I. V. Machado, J. R. N. dos Santos, M. A. P. Januario and A. G. Correea, *Ultrason. Sonochem.*, 2021, **78**, 105704.

19 R. Mathur, K. S. Negi, R. Shrivastava and R. Nair, *RSC Adv.*, 2021, **11**, 1376–1393.

20 Y. Dudognon, J. Rodriguez, T. Constantieux and X. Bugaut, *Eur. J. Org. Chem.*, 2018, 2432–2442.

21 J. Sherwood, *Angew. Chem., Int. Ed.*, 2018, **57**, 14286–14290.

22 J. H. Clark, T. J. Farmer, A. J. Hunt and J. Sherwood, *Int. J. Mol. Sci.*, 2015, **16**, 17101–17159.

23 S. M. Jin, F. Byrne, C. R. McElroy, J. Sherwood, J. H. Clark and A. J. Hunt, *Faraday Discuss.*, 2017, **202**, 157–173.

24 S. Abou-Shehada, J. H. Clark, G. Paggiola and J. Sherwood, *Chem. Eng. Process.*, 2016, **99**, 88–96.

25 C. Liu, X. Huang and J. Li, *Sci. Total Environ.*, 2020, **720**, 137640.

26 A. Jordan, C. G. J. Hall, L. R. Thorp and H. F. Sneddon, *Chem. Rev.*, 2022, **122**, 6749–6794.

27 L. Cicco, G. Dilauro, F. M. Perna, P. Vitale and V. Capriati, *Org. Biomol. Chem.*, 2021, **19**, 2558–2577.

28 F. Gao, R. X. Bai, F. Ferlin, L. Vaccaro, M. H. Li and Y. L. Gu, *Green Chem.*, 2020, **22**, 6240–6257.

29 Y. T. Tan, A. S. M. Chua and G. C. Ngoh, *Bioresour. Technol.*, 2020, **297**, 122522.

30 K. Kohli, R. Prajapati and B. K. Sharma, *Energies*, 2019, **12**, 233.

31 K. Hackl and W. Kunz, *C. R. Chim.*, 2018, **21**, 572–580.

32 F. G. Calvo-Flores, M. J. Monteagudo-Arrebola, J. A. Dobado and J. Isac-Garcia, *Top. Curr. Chem.*, 2018, **376**, 18.

33 J. B. Zimmerman, P. T. Anastas, H. C. Erythropel and W. Leitner, *Science*, 2020, **367**, 397–400.

34 R. A. Sheldon, *Curr. Opin. Green Sustainable Chem.*, 2019, **18**, 13–19.

35 P. Gandeepan, N. Kaplaneris, S. Santoro, L. Vaccaro and L. Ackermann, *ACS Sustainable Chem. Eng.*, 2019, **7**, 8023–8040.

36 S. Santoro, F. Ferlin, L. Luciani, L. Ackermann and L. Vaccaro, *Green Chem.*, 2017, **19**, 1601–1612.

37 F. S. De Oliveira, P. M. De Oliveira, L. M. Farias, R. C. Brinkerhoff, R. Sobrinho, T. M. Treptow, C. R. M. D'Oca, M. A. G. Marinho, M. A. Hort, A. P. Horn, D. Russowsky and M. G. M. D'Oca, *MedChemComm*, 2018, **9**, 1282–1288.

38 G. C. Tron, A. Minassi and G. Appendino, *Eur. J. Org. Chem.*, 2011, 5541–5550.

39 P. Biginelli, *Gazz. Chim. Ital.*, 1891, **21**, 497–500.

40 P. Biginelli, *Gazz. Chim. Ital.*, 1891, **21**, 455–461.

41 P. Biginelli, *Gazz. Chim. Ital.*, 1893, **23**, 360–416.

42 P. Biginelli, *Ber. Dtsch. Chem. Ges.*, 1893, **26**, 447.

43 M. O. Rodrigues, M. N. Eberlin and B. A. D. Neto, *Chem. Rec.*, 2021, **21**, 2762–2781.

44 T. U. Mayer, T. M. Kapoor, S. J. Haggarty, R. W. King, S. L. Schreiber and T. J. Mitchison, *Science*, 1999, **286**, 971–974.

45 M. Matias, G. Campos, A. O. Santos, A. Falcao, S. Silvestre and G. Alves, *RSC Adv.*, 2016, **6**, 84943–84958.

46 V. P. de Souza, F. S. Santos, F. S. Rodembusch, C. B. Braga, C. Ornelas, R. A. Pilli and D. Russowsky, *New J. Chem.*, 2020, **44**, 12440–12451.

47 T. G. M. Treptow, F. Figueiró, E. H. F. Jandrey, A. M. O. Battastini, C. G. Salbego, J. B. Hoppe, P. S. Taborda, S. B. Rosa, L. A. Piovesan, C. D. R. Montes D'Oca, D. Russowsky and M. G. Montes D'Oca, *Eur. J. Med. Chem.*, 2015, **95**, 552–562.

48 F. Figueiro, F. B. Mendes, P. F. Corbelini, F. Janarelli, E. H. Farias Jandrey, D. Russowsky, V. L. Eifler-Lima and A. M. Oliveira Battastini, *Anticancer Res.*, 2014, **34**, 1837–1842.

49 R. F. S. Canto, A. Bernardi, A. M. O. Battastini, D. Russowsky and V. L. Eifler-Lima, *J. Braz. Chem. Soc.*, 2011, **22**, 1379–1388.

50 N. Jankovic, J. T. Ristovski, M. Vranes, A. Tot, J. Petronijevic, N. Joksimovic, T. Stanojkovic, M. D. Crnogorac, N. Petrovic, I. Boljevic, I. Z. Matic, G. A. Bogdanovic, M. Mikov and Z. Bugarcic, *Bioorg. Chem.*, 2019, **86**, 569–582.

51 F. A. R. Barbosa, T. Siminski, R. F. S. Canto, G. M. Almeida, N. S. R. S. Mota, F. Ourique, R. C. Pedrosa and A. L. Braga, *Eur. J. Med. Chem.*, 2018, **155**, 503–515.

52 H. Y. K. Kaan, V. Ulaganathan, O. Rath, H. Prokopcova, D. Dallinger, C. O. Kappe and F. Kozielski, *J. Med. Chem.*, 2010, **53**, 5676–5683.

3648 | *Org. Biomol. Chem.*, 2024, **22**, 3630–3651

This journal is © The Royal Society of Chemistry 2024

53 G. Lauro, M. Strocchia, S. Terracciano, I. Bruno, K. Fischer, C. Pergola, O. Werz, R. Riccio and G. Bifulco, *Eur. J. Med. Chem.*, 2014, **80**, 407–415.

54 K. V. Sashidhara, S. R. Avula, K. Sharma, G. R. Palnati and S. R. Bathula, *Eur. J. Med. Chem.*, 2013, **60**, 120–127.

55 D. L. da Silva, F. S. Reis, D. R. Muniz, A. Ruiz, J. E. de Carvalho, A. A. Sabino, L. V. Modolo and A. de Fatima, *Bioorg. Med. Chem.*, 2012, **20**, 2645–2650.

56 M. Marinescu, *Molecules*, 2021, **26**, 6022.

57 H. Nagarajaiah, A. Mukhopadhyay and J. N. Moorthy, *Tetrahedron Lett.*, 2016, **57**, 5135–5149.

58 B. A. D. Neto, T. A. Fernandes and M. V. Correia, in *Targets Heterocycl. Syst*, 2018, vol. 22, pp. 356–376.

59 C. O. Kappe, *Eur. J. Med. Chem.*, 2000, **35**, 1043–1052.

60 C. O. Kappe, *Tetrahedron*, 1993, **49**, 6937–6963.

61 C. O. Kappe, *Acc. Chem. Res.*, 2000, **33**, 879–888.

62 P. Costanzo, M. Nardi and M. Oliverio, *Eur. J. Org. Chem.*, 2020, 3954–3964.

63 A. V. Smolobochkin, A. S. Gazizov, A. R. Burilov, M. A. Pudovik and O. G. Sinyashin, *Russ. Chem. Rev.*, 2021, **90**, 395–417.

64 M. M. Heravi and V. Zadsirjan, *Curr. Org. Chem.*, 2020, **24**, 1331–1366.

65 A. M. A. Shumaila and A. A. N. Al-Thulaia, *Synth. Commun.*, 2019, **49**, 1613–1632.

66 C. O. Kappe, *QSAR Comb. Sci.*, 2003, **22**, 630–645.

67 S. Y. Yu, J. X. Wu, H. B. Lan, L. H. Gao, H. Y. Qian, K. Q. Fan and Z. G. Yin, *Org. Lett.*, 2020, **22**, 102–105.

68 M. Stucchi, G. Lesma, F. Meneghetti, G. Rainoldi, A. Sacchetti and A. Silvani, *J. Org. Chem.*, 2016, **81**, 1877–1884.

69 S. Z. D. Heirati, F. Shirini and A. F. Shojaei, *RSC Adv.*, 2016, **6**, 67072–67085.

70 J. Safari, S. Gandomi-Ravandi and S. Ashiri, *New J. Chem.*, 2016, **40**, 512–520.

71 M. Nasr-Esfahani and M. Taei, *RSC Adv.*, 2015, **5**, 44978–44989.

72 Y. V. Sedash, N. Y. Gorobets, V. A. Chebanov, I. S. Konovalova, O. V. Shishkin and S. M. Desenko, *RSC Adv.*, 2012, **2**, 6719–6728.

73 A. Shaabani, M. Seyyedhamzeh, A. Maleki and F. Hajishaabanha, *Tetrahedron*, 2010, **66**, 4040–4042.

74 N. Y. Gorobets, Y. V. Sedash, K. S. Ostras, O. V. Zaremba, S. V. Shishkina, V. N. Baumer, O. V. Shishkin, S. M. Kovalenko, S. M. Desenko and E. V. Van der Eycken, *Tetrahedron Lett.*, 2010, **51**, 2095–2098.

75 N. Li, X. H. Chen, J. Song, S. W. Luo, W. Fan and L. Z. Gong, *J. Am. Chem. Soc.*, 2009, **131**, 15301–15310.

76 Z. T. Wang, L. W. Xu, C. G. Xia and H. Q. Wang, *Tetrahedron Lett.*, 2006, **47**, 1361–1361.

77 M. M. Abelman, S. C. Smith and D. R. James, *Tetrahedron Lett.*, 2003, **44**, 4559–4562.

78 B. C. Oreilly and K. S. Atwal, *Heterocycles*, 1987, **26**, 1185–1188.

79 K. S. Atwal, B. C. Oreilly, J. Z. Gougoutas and M. F. Malley, *Heterocycles*, 1987, **26**, 1189–1192.

80 K. S. Atwal, G. C. Rovnyak, J. Schwartz, S. Moreland, A. Hedberg, J. Z. Gougoutas, M. F. Malley and D. M. Floyd, *J. Med. Chem.*, 1990, **33**, 1510–1515.

81 K. S. Atwal, G. C. Rovnyak, B. C. Oreilly and J. Schwartz, *J. Org. Chem.*, 1989, **54**, 5898–5907.

82 M. R. Bhosle, D. B. Wahul, G. M. Bondle, A. Sarkate and S. V. Tiwari, *Synth. Commun.*, 2018, **48**, 2046–2060.

83 D. Parthiban, *J. Heterocycl. Chem.*, 2023, **60**, 1210–1222.

84 P. K. Sahu, P. K. Sahu, M. S. Kaurav, M. Messali, S. M. Almutairi, P. L. Sahu and D. D. Agarwal, *ACS Omega*, 2018, **3**, 15035–15042.

85 P. K. Sahu, P. K. Sahu, M. S. Kaurav, M. Messali, S. M. Almutairi, P. L. Sahu and D. D. Agarwal, *RSC Adv.*, 2018, **8**, 33952–33959.

86 M. S. Kaurav, P. K. Sahu, P. K. Sahu, M. Messali, S. M. Almutairi, P. L. Sahu and D. D. Agarwal, *RSC Adv.*, 2019, **9**, 3755–3763.

87 J. Puvithra and D. Parthiban, *Asian J. Chem.*, 2020, **32**, 2067–2074.

88 S. Sadjadi, M. M. Heravi, V. Zadsirjan, S. Y. S. Beheshtiha and R. R. Kelishadi, *ChemistrySelect*, 2018, **3**, 12031–12038.

89 S. Abdolmohammadi and S. Karimpour, *Chin. Chem. Lett.*, 2016, **27**, 114–118.

90 M. M. Heravi, T. Hosseinnejad, M. Tamimi, V. Zadsirjan and M. Mirzaei, *J. Mol. Struct.*, 2020, **1205**, 127598.

91 H. Mehrabi and M. Baniasad-Dashtabi, *J. Chem. Res.*, 2015, 294–295.

92 P. K. Ambre, R. R. S. Pissurlenkar, R. D. Wavhale, M. S. Shaikh, V. M. Khedkar, B. Wan, S. G. Franzblau and E. C. Coutinho, *Med. Chem. Res.*, 2014, **23**, 2564–2575.

93 Y. I. Shaikh, S. S. Shaikh, K. Ahmed, G. M. Nazeruddin and V. S. Shaikh, *Orient. J. Chem.*, 2020, **36**, 415–418.

94 Z. N. Siddiqui and T. Khan, *RSC Adv.*, 2014, **4**, 2526–2537.

95 M. Kidwai, S. Saxena and R. Mohan, *Russ. J. Org. Chem.*, 2006, **42**, 52–55.

96 G. Sabitha, G. Reddy, K. B. Reddy and J. S. Yadav, *Tetrahedron Lett.*, 2003, **44**, 6497–6499.

97 D. W. Song, G. L. Liu, M. Y. Xue, T. X. Qiu, H. Wang, L. P. Shan, L. Liu and J. Chen, *Virus Res.*, 2021, **291**, 198221.

98 F. Ghobakhloo, D. Azarifar and M. Mohammadi, *J. Phys. Chem. Solids*, 2023, **175**, 111222.

99 Z. Besharati, M. Malmir and M. M. Heravi, *Inorg. Chem. Commun.*, 2022, **143**, 109813.

100 A. K. Bhagi, K. P. Singh, A. Kumar, Priya and N. Manav, *Indian J. Chem.*, 2022, **61**, 1173–1179.

101 S. Sadjadi, M. M. Heravi and M. Malmir, *Res. Chem. Intermed.*, 2017, **43**, 6701–6717.

102 P. Ghamari Kargar and G. Bagherzade, *Sci. Rep.*, 2023, **13**, 19104.

103 G. Brahmachari and K. Nurjamal, *ChemistrySelect*, 2017, **2**, 3695–3702.

104 L. Zare Fekri, M. Nikpassand and S. Pourmirzajani, *Org. Prep. Proced. Int.*, 2020, **52**, 396–401.

This journal is © The Royal Society of Chemistry 2024

Org. Biomol. Chem., 2024, **22**, 3630–3651 | **3649**

105 L. Z. Fekri, M. Nikpassand, S. Pourmirzajani and B. Aghazadeh, *RSC Adv.*, 2018, **8**, 22313–22320.

106 A. N. Nadaf and K. Shivashankar, *Synth. Commun.*, 2018, **48**, 809–815.

107 B. A. D. Neto, R. O. Rocha and A. A. M. Lapis, *Curr. Opin. Green Sustainable Chem.*, 2022, **35**, 100608.

108 H. Ben Salah, P. Nancarrow and A. Al-Othman, *Fuel*, 2021, **302**, 121195.

109 N. V. Plechkova and K. R. Seddon, *Chem. Soc. Rev.*, 2008, **37**, 123–150.

110 N. Dib, C. M. O. Lepori, N. M. Correa, J. J. Silber, R. D. Falcone and L. Garcia-Rio, *Polymers*, 2021, **13**, 1378.

111 M. Atilhan and S. Aparicio, *J. Pet. Sci. Eng.*, 2021, **205**, 108746.

112 G. A. S. Haron, H. Mahmood, M. H. Noh, M. Z. Alam and M. Moniruzzaman, *ACS Sustainable Chem. Eng.*, 2021, **9**, 1008–1034.

113 K. S. Khoo, X. F. Tan, C. W. Ooi, K. W. Chew, W. H. Leong, Y. H. Chai, S. H. Ho and P. L. Show, *J. Cleaner Prod.*, 2021, **284**, 124772.

114 T. U. Rashid, *J. Mol. Liq.*, 2021, **321**, 114916.

115 P. A. Z. Suarez and H. F. Ramalho, *Curr. Org. Chem.*, 2013, **17**, 229–237.

116 B. A. D. Neto, P. S. Beck, J. E. P. Sorto and M. N. Eberlin, *Molecules*, 2022, **27**, 7552.

117 R. W. Taft, J. L. M. Abboud, M. J. Kamlet and M. H. Abraham, *J. Solution Chem.*, 1985, **14**, 153–186.

118 M. J. Kamlet, J. L. Abboud and R. W. Taft, *J. Am. Chem. Soc.*, 1977, **99**, 6027–6038.

119 R. W. Taft and M. J. Kamlet, *J. Am. Chem. Soc.*, 1976, **98**, 2886–2894.

120 M. J. Kamlet and R. W. Taft, *J. Am. Chem. Soc.*, 1976, **98**, 377–383.

121 R. A. Sheldon, *Chem. Commun.*, 2008, 3352–3365.

122 R. A. Sheldon, *Green Chem.*, 2007, **9**, 1273–1283.

123 R. A. Sheldon, *C. R. Acad. Sci., Ser. IIc: Chim.*, 2000, **3**, 541–551.

124 L. G. do Nascimento, I. M. Dias, G. B. M. de Souza, I. Dancini-Pontes, N. R. C. Fernandes, P. S. de Souza, G. R. de Oliveira and C. G. Alonso, *J. Org. Chem.*, 2020, **85**, 11170–11180.

125 I. L. Goncalves, L. Davi, L. Rockenbach, G. M. das Neves, L. P. Kagami, R. F. Santos Canto, F. Figueiro, A. M. Oliveira Battastini and V. L. Eifler-Lima, *Tetrahedron Lett.*, 2018, **59**, 2759–2762.

126 W. G. Fan, Y. Queneau and F. Popowycz, *Green Chem.*, 2018, **20**, 485–492.

127 V. J. Lillo and J. M. Saa, *Chem. – Eur. J.*, 2016, **22**, 17182–17186.

128 J.-H. Wang, G.-M. Tang, Y.-T. Wang, Y.-Z. Cui, J.-J. Wang and S. W. Ng, *Dalton Trans.*, 2015, **44**, 17829–17840.

129 Q. Zhang, X. Wang, Z. Li, W. Wu, J. Liu, H. Wu, S. Cui and K. Guo, *RSC Adv.*, 2014, **4**, 19710–19715.

130 B. Karimi, A. Mobaraki, H. M. Mirzaei, D. Zareyee and H. Vali, *ChemCatChem*, 2014, **6**, 212–219.

131 A. M. Zafar, S. Qureshi, M. N. Khan, M. Azad, M. A. Munawar and M. A. Khan, *Asian J. Chem.*, 2013, **25**, 3244–3246.

132 M. Dewan, A. Kumar, A. Saxena, A. De and S. Mozumdar, *PLoS One*, 2012, **7**, e43078.

133 M. N. Godoi, H. S. Costenaro, E. Kramer, P. S. Machado, M. G. Montes D'Oca and D. Russowsky, *Quim. Nova*, 2005, **28**, 1010–1013.

134 D. Russowsky, F. A. Lopes, V. S. S. da Silva, K. F. S. Canto, M. G. M. D'Oca and M. N. Godoi, *J. Braz. Chem. Soc.*, 2004, **15**, 165–169.

135 T. N. Tejero, A. E. Kummerle and G. F. Bauerfeldt, *Rev. Virtual Quim.*, 2019, **11**, 1203–1224.

136 V. F. Traven, V. V. Negrebetsky, L. I. Vorobjeva and E. A. Carberry, *Can. J. Chem.*, 1997, **75**, 377–383.

137 C. R. Reddy, N. Kiranmai, K. Johny, M. Pendke and P. Naresh, *Synthesis*, 2009, 399–402.

138 F. F. Wolf, H. Klare and B. Goldfuss, *J. Org. Chem.*, 2016, **81**, 1762–1768.

139 M. M. Abdou, R. A. El-Saeed and S. Bondock, *Arabian J. Chem.*, 2019, **12**, 974–1003.

140 M. M. Abdou, R. A. El-Saeed and S. Bondock, *Arabian J. Chem.*, 2019, **12**, 88–121.

141 G. M. Ziarani, R. Moradi, T. Ahmadi and P. Gholamzadeh, *Mol. Divers.*, 2019, **23**, 1029–1064.

142 A. Benazzouz, M. Makhloufi-Chebli, N. Khatir-Hamdi, B. Boutemeur-Khedis, A. M. S. Silva and M. Hamdi, *Tetrahedron*, 2015, **71**, 3890–3894.

143 H. Saffarian, F. Karimi, M. Yarie and M. A. Zolfigol, *J. Mol. Struct.*, 2021, **1224**, 129294.

144 E. Priede, S. Brica, E. Bakis, N. Udris and A. Zicmanis, *New J. Chem.*, 2015, **39**, 9132–9142.

145 D. J. Macquarrie, J. H. Clark, A. Lambert, J. E. G. Mdoe and A. Priest, *React. Funct. Polym.*, 1997, **35**, 153–158.

146 A. Ray, T. Bristow, C. Whitmore and J. Mosely, *Mass Spectrom. Rev.*, 2018, **37**, 565–579.

147 A. J. Ingram, C. L. Boeser and R. N. Zare, *Chem. Sci.*, 2016, **7**, 39–55.

148 C. Iacobucci, S. Reale and F. De Angelis, *Angew. Chem., Int. Ed.*, 2016, **55**, 2980–2993.

149 C.-C. Chen and P.-C. Lin, *Anal. Methods*, 2015, **7**, 6947–6959.

150 J. Limberger, B. C. Leal, A. L. Monteiro and J. Dupont, *Chem. Sci.*, 2015, **6**, 77–94.

151 M. Matache, C. Dobrota, N. D. Bogdan, I. Dumitru, L. L. Ruta, C. C. Paraschivescu, I. C. Farcasanu, I. Baciu and D. P. Funeriu, *Tetrahedron*, 2009, **65**, 5949–5957.

152 D. Kumar, F. Malik, P. M. S. Bedi and S. Jain, *Chem. Pharm. Bull.*, 2016, **64**, 399–409.

153 Q. Ren, J. Kang, M. Li, L. Yuan, R. Chen and L. Wang, *Eur. J. Org. Chem.*, 2017, 5566–5571.

154 Z. He, X. Lin, Y. Zhu and Y. Wang, *Heterocycles*, 2010, **81**, 965–976.

155 S. Yang, L.-l. Shen, Y.-J. Kim and J.-H. Jeong, *Org. Biomol. Chem.*, 2016, **14**, 623–630.

156 M. Lashkari, M. Ghashang and A. Abedi-Madiseh, *Org. Prep. Proced. Int.*, 2020, **53**, 52–58.

157 Z. Karimi-Jaberi, B. Masoudi, A. Rahmani and K. Alborzi, *Polycyclic Aromat. Compd.*, 2020, **40**, 99–107.

158 M. Gohain, J. H. van Tonder and B. C. B. Bezuidenhoudt, *Tetrahedron Lett.*, 2013, **54**, 3773–3776.

159 S. Yaragorla, P. L. Saini and G. Singh, *Tetrahedron Lett.*, 2015, **56**, 1649–1653.

160 G. Brahmachari and B. Banerjee, *ACS Sustainable Chem. Eng.*, 2014, **2**, 411–422.

161 J. Tiwari, M. Saquib, S. Singh, F. Tufail, M. Singh, J. Singh and J. Singh, *Green Chem.*, 2016, **18**, 3221–3231.

162 G. Zhang, Y. Zhang, J. Yan, R. Chen, S. Wang, Y. Ma and R. Wang, *J. Org. Chem.*, 2012, **77**, 878–888.

163 Z. Chen, Q. Zhu and W. Su, *Tetrahedron Lett.*, 2011, **52**, 2601–2604.

164 M. Khalaj, *Arabian J. Chem.*, 2020, **13**, 6403–6411.

165 N. Basirat, S. S. Sajadikhah and A. Zare, *Res. Chem. Intermed.*, 2020, **46**, 3263–3275.

166 N. Basirat, *Res. Chem. Intermed.*, 2020, **46**, 5441–5458.

167 P. K. Sahu, *RSC Adv.*, 2016, **6**, 78409–78423.

168 P. K. Sahu, *RSC Adv.*, 2016, **6**, 67651–67661.

169 S. Hosseinzadegan, N. Hazeri and M. T. Maghsoodlou, *Appl. Organomet. Chem.*, 2020, **34**, e5797.

170 P. Kisszekelyi, A. Alammar, J. Kupai, P. Huszthy, J. Barabas, T. Holtzl, L. Szente, C. Bawn, R. Adams and G. Szekely, *J. Catal.*, 2019, **371**, 255–261.

171 A. Zgrzeba, E. Andrzejewska and A. Marcinkowska, *RSC Adv.*, 2015, **5**, 100354–100361.

172 K. A. Nolan, J. R. Doncaster, M. S. Dunstan, K. A. Scott, A. D. Frenkel, D. Siegel, D. Ross, J. Barnes, C. Levy, D. Leys, R. C. Whitehead, I. J. Stratford and R. A. Bryce, *J. Med. Chem.*, 2009, **52**, 7142–7156.

173 E. Rostami and S. H. Zare, *ChemistrySelect*, 2019, **4**, 13295–13303.

174 F. G. Medina, J. G. Marrero, M. Macias-Alonso, M. C. Gonzalez, I. Cordova-Guerrero, A. G. T. Garcia and S. Osegueda-Roblesa, *Nat. Prod. Rep.*, 2015, **32**, 1472–1507.

175 P. B. Pansuriya and M. N. Patel, *Appl. Organomet. Chem.*, 2007, **21**, 719–727.

176 D. Simijonovic, E. E. Vlachou, Z. D. Petrovic, D. J. Hadjipavlou-Litina, K. E. Litinas, N. Stankovic, N. Mihovic and M. P. Mladenovic, *Bioorg. Chem.*, 2018, **80**, 741–752.

177 H. Bavandi, Z. Habibi and M. Yousefi, *Bioorg. Chem.*, 2020, **103**, 104139.

178 J. Han, L. D. Sun, Y. Y. Chu, Z. Li, D. D. Huang, X. Y. Zhu, H. Qian and W. L. Huang, *J. Med. Chem.*, 2013, **56**, 9955–9968.

179 C. Sun, W. Zhao, X. Wang, Y. Sun and X. Chen, *Pharmacol. Res.*, 2020, **160**, 105193.

180 K. Kajal, R. Shakya, M. Rashid, V. Nigam, B. D. Kurmi, G. D. Gupta and P. Patel, *Sustainable Chem. Pharm.*, 2024, **37**, 101374.

181 F. A. Macías, D. Castellano and J. M. G. Molinillo, *J. Agric. Food Chem.*, 2000, **48**, 2512–2521.

182 S. M. Potdar, A. R. Deshmukh and K. T. Waghmode, *Lett. Org. Chem.*, 2021, **18**, 924–927.

183 D. Russowsky, R. F. S. Canto, S. A. A. Sanches, M. G. M. D'Oca, A. de Fatima, R. A. Pilli, L. K. Kohn, M. A. Antonio and J. E. de Carvalho, *Bioorg. Chem.*, 2006, **34**, 173–182.

184 T. E. Balius, S. Mukherjee and R. C. Rizzo, *J. Comput. Chem.*, 2011, **32**, 2273–2289.

185 S. R. Brozell, S. Mukherjee, T. E. Balius, D. R. Roe, D. A. Case and R. C. Rizzo, *J. Comput.-Aided Mol. Des.*, 2012, **26**, 749–773.

186 Y. Yan, V. Sardana, B. Xu, C. Homnick, W. Halczenko, C. A. Buser, M. Schaber, G. D. Hartman, H. E. Huber and L. C. Kuo, *J. Mol. Biol.*, 2004, **335**, 547–554.

187 J. P. M. Jämbeck and A. P. Lyubartsev, *J. Phys. Chem. B*, 2014, **118**, 3793–3804.

188 J. Wang, R. M. Wolf, J. W. Caldwell, P. A. Kollman and D. A. Case, *J. Comput. Chem.*, 2004, **25**, 1157–1174.

189 A. Jakalian, B. L. Bush, D. B. Jack and C. I. Bayly, *J. Comput. Chem.*, 2000, **21**, 132–146.

190 A. Jakalian, D. B. Jack and C. I. Bayly, *J. Comput. Chem.*, 2002, **23**, 1623–1641.

191 D. A. Case, H. M. Aktulga, K. Belfon, D. S. Cerutti, G. A. Cisneros, V. W. D. Cruzeiro, N. Forouzesh, T. J. Giese, A. W. Götz, H. Gohlke, S. Izadi, K. Kasavajhala, M. C. Kaymak, E. King, T. Kurtzman, T.-S. Lee, P. Li, J. Liu, T. Luchko, R. Luo, M. Manathunga, M. R. Machado, H. M. Nguyen, K. A. O'Hearn, A. V. Onufriev, F. Pan, S. Pantano, R. Qi, A. Rahnamoun, A. Risheh, S. Schott-Verdugo, A. Shajan, J. Swails, J. Wang, H. Wei, X. Wu, Y. Wu, S. Zhang, S. Zhao, Q. Zhu, T. E. Cheatham III, D. R. Roe, A. Roitberg, C. Simmerling, D. M. York, M. C. Nagan and K. M. Merz, Jr., *J. Chem. Inf. Model.*, 2023, **63**, 6183–6191.

192 J. Wang, W. Wang, P. A. Kollman and D. A. Case, *J. Mol. Graphics Modell.*, 2006, **25**, 247–260.

193 J. A. Maier, C. Martinez, K. Kasavajhala, L. Wickstrom, K. E. Hauser and C. Simmerling, *J. Chem. Theory Comput.*, 2015, **11**, 3696–3713.

194 P. Mark and L. Nilsson, *J. Phys. Chem. A*, 2001, **105**, 9954–9960.

195 M. R. Shirts, C. Klein, J. M. Swails, J. Yin, M. K. Gilson, D. L. Mobley, D. A. Case and E. D. Zhong, *Comput. Aided Mol. Des.*, 2017, **31**, 147–161.

196 UCSF Computer Graphics Laboratory, San Francisco, CA, 2003.

197 R. L. DesJarlais, R. P. Sheridan, G. L. Seibel, J. S. Dixon, I. D. Kuntz and R. Venkataraghavan, *J. Med. Chem.*, 1988, **31**, 722–729.

198 E. C. Meng, B. K. Shoichet and I. D. Kuntz, *J. Comput. Chem.*, 1992, **13**, 505–524.

This journal is © The Royal Society of Chemistry 2024

Org. Biomol. Chem., 2024, **22**, 3630–3651 | **3651**